LP1-mPAH) has been described previously [9]. 1×10^{11} vector genomes of the recombinant AAV were dissolved in 0.5 ml of saline and injected into the peritoneal cavity of a PKU mouse at 8 weeks of age.

Brain sampling and biochemical analysis

Mice were killed by cervical dislocation, and the removed brain was immediately frozen in liquid nitrogen and stored at −80°C until used. The brain was homogenized in 10 volumes of 0.2 M of perchloric acid containing 0.1 mM of EDTA for deproteination. Protein concentrations were determined using a DC protein assay kit (Bio-Rad, Hercules, California, USA). Catecholamine and 5-HT levels were measured by high-performance liquid chromatography using an electrochemical detector ECD-100 (EICOM, Kyoto, Japan) as described elsewhere [12]. Amino acid levels were analyzed using an L-8500 amino acid analyzer (Hitachi, Tokyo, Japan). Data are presented as means ± SDs in the text and figures. An unpaired *t*-test was performed using the StatView 5.0 software for Macintosh (SAS Institute, Cary, North Carolina, USA) for comparison between two groups, and a *P* value of less than 0.05 was considered to be significant.

Results

Phenotypic correction after gene transfer

As shown in the original BTBR-*Pah*^{enu2} mice [9], the scAAV8/LP1-mPAH vector exhibited remarkable efficacy in restoring phenylalanine catabolism in C57BL/6-*Pah*^{enu2} mice. Before the gene transfer, PKU mice had elevated blood phenylalanine levels (28.1 ± 1.7 mg/dl; $n = 3$) compared with their heterozygous (+/−) littermates (0.3 ± 0.2 mg/dl; $n = 6$), whereas blood phenylalanine levels in heterozygous mice were indistinguishable from those in wild-type homozygous (WT, +/+) mice (0.3 ± 0.1 mg/dl; $n = 6$). After a single injection of the AAV vector to PKU mice, the blood phenylalanine concentration rapidly decreased to a near-normal level in 1 week (1.7 ± 0.8 mg/dl) and remained within the normal range from weeks 2 to 8 (Fig. 1a). In parallel, we evaluated phenylalanine-oxidizing capacity by conducting a ^{13}C-phenylalanine-loading breath test (Fig. 1b). In this assay, the production of $^{13}CO_2$ (ΔCO_2) is associated with PAH activity, although we were not able to distinguish heterozygous mice (50.6 ± 6.7‰; $n = 6$) from WT mice (52.6 ± 10.5‰; $n = 6$), presumably due to other limiting factors such as phenylalanine transport and cofactor availability *in vivo*. Before the gene transfer, PKU mice produced very little, if any, ΔCO_2 (2.0 ± 1.1‰; $n = 3$). One week post-AAV injection, ΔCO_2 was increased to 2/3 of the control level (29.9 ± 1.1‰) and the value gradually increased to a near-normal level (41.8 ± 3.5‰ at week 8).

The AAV-treated PKU mice ($n = 3$) were euthanized at week 8 after injection along with heterozygous littermates ($n = 6$) and age-matched, untreated PKU mice ($n = 4$) for further analysis. First, we measured the whole brain weight of these animals (Fig. 1c). As reported [13], the weight of the brain in untreated PKU mice was significantly decreased compared with the control level (343 ± 15 vs. 481 ± 33 mg; $P = 0.00005$). In contrast, the brains of AAV-treated PKU animals regained weight significantly (431 ± 26 mg; $P = 0.0023$ vs. untreated PKU), reaching a level comparable level to that in heterozygous mice ($P = 0.55$).

Amino acid analysis

In the amino acid analysis, we confirmed that the untreated PKU mice had a marked imbalance of phenylalanine and tyrosine in the brain [13] (Fig. 2a). The phenylalanine content was nearly 10 times that of heterozygous mice (6.24 ± 0.81 vs. 0.66 ± 0.08 nmol/mg protein; $P = 0.0008$), whereas the tyrosine content was lower (0.31 ± 0.08 vs. 0.77 ± 0.09 nmol/mg protein; $P = 0.0005$). In the AAV-treated PKU mice, the amount of phenylalanine in the

Fig. 1

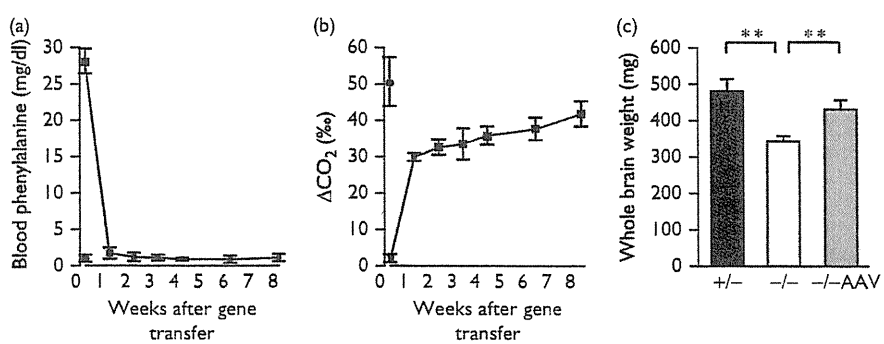

Phenotypic correction in phenylketonuria (PKU) mice after gene transfer. (a) Blood phenylalanine levels in adeno-associated virus (AAV)-treated PKU mice (squares) and heterozygous controls (circle). (b) $^{13}CO_2$ production (ΔCO_2) by AAV-treated PKU mice (squares) and heterozygous controls (circle) in a [1-^{13}C]L-phenylalanine-loading test. (c) Whole brain weights of heterozygous control (+/−), untreated PKU (−/−), and AAV-treated PKU (−/−AAV) mice. Data are shown as the mean ± SD. **P<0.01.

brain was decreased (1.04 ± 0.50 nmol/mg of protein; $P = 0.001$ vs. untreated PKU) in accordance with that in blood. The treated mice also had increased levels of tyrosine, but the elevation was not significant because one animal had a supranormal tyrosine content (1.55 nmol/mg of protein) that resulted in a relatively large SD for this group. As for tryptophan, the untreated PKU mice had a lower average level (0.12 ± 0.05 nmol/mg protein) than the heterozygous and AAV-treated mice (0.21 ± 0.11 and 0.28 ± 0.13 nmol/mg of protein, respectively), but the difference was not significant as reported previously [7].

Monoamine neurotransmitters and metabolites

The levels of catecholamines, serotonin, and metabolites are summarized in Table 1. We confirmed that the amounts of dopamine, norepinephrine, and 5-HT in the untreated PKU mice were significantly decreased compared with those in the heterozygous controls ($P = 0.004$, 0.0005, and 0.00008, respectively) [6,7]. Eight weeks after gene transfer, such aminergic deficits were markedly ameliorated ($P = 0.022$, 0.0007, and 0.0004 vs. untreated PKU, respectively; Fig. 2b). Accordingly, the levels of some catecholamine metabolites increased in the AAV-treated mice. In PKU mice, 3-4-dihydroxyphenylacetic acid decreased significantly compared with the heterozygous controls, and it recovered partly after gene transfer. 3-methoxytyramine (3-MT) content in PKU mice was not significantly lower than that in the heterozygous controls, but it may have actually been lower compared with WT homozygotes [6]. Otherwise, a compensatory dopamine release to the synapse may take place in PKU mice, resulting in a relatively small 3-MT decrease. As shown in Table 1, we found a significant increase in 3-MT after gene therapy, presumably due to an improved dopamine synthesis. In contrast, homovanillic acid did not increase after gene transfer ($P = 0.749$ vs. PKU; $P = 0.023$ vs. heterozygous). Overall, we assumed that catecholamine synthesis in the AAV-treated mice was restored to approximately 80–90% of the level in heterozygous mice. Similarly, the levels of serotonin and its metabolite 5-hydroxyindoleacetic acid recovered to 60–70% of those in heterozygous mice ($P = 0.039$ for 5-HT and $P = 0.092$ for 5-hydroxyindoleacetic acid).

Fig. 2

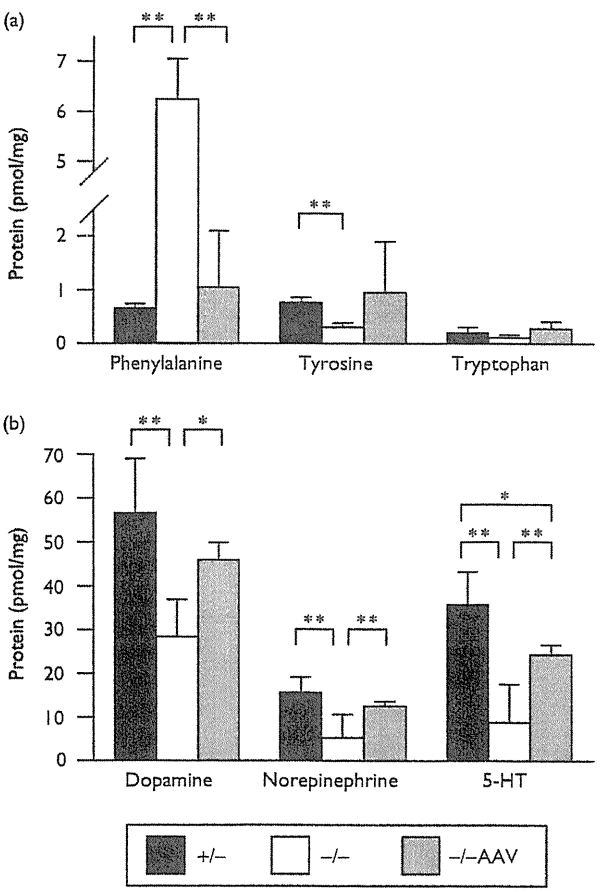

Aromatic amino acids and neurogenic amines in the phenylketonuria (PKU) mouse brain. (a) Phenylalanine, tyrosine, and tryptophan levels in the brain of heterozygous control (+/−), untreated PKU (−/−), and adeno-associated virus (AAV)-treated PKU (−/−AAV) mice. (b) Dopamine, norepinephrine, and serotonin (5-HT) levels in the brain of heterozygous control (+/−), untreated PKU (−/−), and AAV-treated PKU (−/−AAV) mice. Data are shown as the mean ± SD. *$P<0.05$, **$P<0.01$.

Discussion

The present study showed an overt reversal of the aminergic deficit in PKU mouse brain after liver-targeted gene therapy. In untreated PKU mice, HPA may disturb monoamine synthesis through at least two mechanisms. One is that excess phenylalanine may hamper the neuronal uptake of tyrosine (dopamine and norepinephrine precursor) and tryptophan (5-HT precursor) through competition for transport across the blood–brain barrier by the L-type amino acid carrier [14,15]. The other is that a high concentration of phenylalanine interferes with tyrosine hydroxylase and tryptophan hydroxylase [16,17]. For the catecholamine pathway, we observed a significant decrease in the amount of tyrosine in PKU mice, which may play some role in the dopamine and norepinephrine deficit. However, Joseph and Dyer [18] reported an increase in dopamine despite low tyrosine levels in PKU mice on a low-phenylalanine diet, which may suggest that HPA causes a lack of catecholamine primarily by inhibiting the hydroxylation of tyrosine. As for the serotonin pathway, we found a limited decrease in tryptophan in the PKU mouse brain. Pascucci *et al.* [7] found a similar decrease in tryptophan and observed a significant decrease in 5-hydroxytryptophan in the brain of PKU mice. Therefore, they speculated that HPA impedes 5-HT synthesis mainly by inhibiting tryptophan hydroxylation, which is the rate-limiting step in this pathway. We previously showed that phenylalanine acted as an inhibitor more strongly against tryptophan hydroxylase than against tyrosine hydroxylase [17], further

Table 1 Dopamine, norepinephrine, 5-hydroxytryptamine, and metabolites (pmol/mg protein) in adeno-associated virus-treated *Pah*$^{enu2/enu2}$ and control mouse brain

	Pah$^{enu2/+}$ ($n=6$)	*Pah*$^{enu2/enu2}$ ($n=4$)	*Pah*$^{enu2/enu2}$ + adeno-associated virus ($n=3$)
Dopamine	56.6±12.4[a]	28.4±8.5	45.9 ±4.0[a]
3-Methoxytyramine	11.9±4.6	9.9±2.1	13.7±1.2[b]
3-4-Dihydroxyphenylacetic acid	10.4±2.2[a]	4.7±1.2	7.9±1.6[b]
Homovanillic acid	41.9±12.1[b]	25.1±5.1	26.2±2.7[c]
Norepinephrine	15.7±3.5[a]	5.3±1.4	12.5±1.1[a]
5-Hydroxytryptamine	35.8±7.5[a]	8.8±2.5	24.3±2.3[a,c]
5-Hydroxyindoleacetic acid	24.3±7.9[a]	5.3±1.5	15.0±2.0[a]

Values are represented as mean±SD.
[a]$P<0.01$ vs. *Pah*$^{enu2/enu2}$.
[b]$P<0.05$ vs. *Pah*$^{enu2/enu2}$.
[c]$P<0.05$ vs. *Pah*$^{enu2/+}$.

supporting their speculation. By either mechanism, correction of HPA would reset amine metabolism and thereby improve the relevant brain function, as we demonstrated here and previously [8].

Untreated PKU patients have smaller brains, and the primary pathologic finding is hypomyelination and gliosis of central nervous system white matter. A similar pathologic change is observed in *Pah*^{enu2} mice, which may result from aberrant glial cell differentiation induced by HPA [19]. It has also been documented that cerebral protein synthesis is decreased in PKU mice, which presumably contributes to the underdevelopment and degeneration of the PKU brain [13]. We observed a marked recovery in brain weight in the PKU mice only 8 weeks after gene transfer. Correction of HPA may facilitate protein synthesis and reset glial cell plasticity to reconstitute myelin. In addition, it may reduce oxidative stress and induce neuronal regeneration as shown by Embury *et al.* [20].

The results demonstrate that liver-targeted gene therapy for PKU would restore the structural and biochemical fitness of the brain. Current gene transfer technology has achieved a partial reconstitution of coagulation factor IX in the human liver to ameliorate hemophilia B [21]. Further development should lead to broader applications of this modality including PKU. Preventing HPA without a restrictive diet would make it easier to meet nutritional requirements for the physical and neuronal development of patients as well as to maintain sociopsychological well-being.

Conclusion

Liver-targeted gene therapy for PKU reverses the aminergic deficit in the brain and improves the neuropsychological function.

Acknowledgements

The authors thank Mr. Sho Shimaguchi (Tokyo Institute of Technology) for assisting with brain amine analysis and Prof. Kazunao Kondo (Fujita Health University) for assisting with amino acid analysis. They also thank Prof. Hiroyuki Yoshikawa and Dr. Hiromi Hamada (University of Tsukuba) for enthusiastic support and thoughtful discussion. This work was supported in part by Grants-in-Aid for Scientific Research from the Ministry of Education, Culture, Sports, Science and Technology, Japan (20591230).

Conflicts of interest

There are no conflicts of interest.

References

1 Scriver CR, Kaufman S. Hyperphenylalaninemia: phenylalanine hydroxylase deficiency. In: Scriver CR, Beaudet AL, Sly WS, Valle D, editors. *The metabolic and molecular bases of inherited disease*. 8th ed New York: McGraw-Hill. 2001; pp. 1667–1724.
2 McKean CM. The effects of high phenylalanine concentrations on serotonin and catecholamine metabolism in the human brain. *Brain Res* 1972; **47**:469–476.
3 Güttler F, Lou H. Dietary problems of phenylketonuria: effect on CNS transmitters and their possible role in behavior and neuropsychological function. *J Inherit Metab Dis* 1986; **9 (Suppl 2)**:169–177.
4 Shedlovsky A, McDonald JD, Symula D, Dove WF. Mouse models of human phenylketonuria. *Genetics* 1993; **134**:1205–1210.
5 McDonald JD, Charlton CK. Characterization of mutations at the mouse phenylalanine hydroxylase locus. *Genomics* 1997; **39**:402–405.
6 Puglisi-Allegra S, Cabib S, Pascucci T, Ventura R, Cali F, Romano V. Dramatic brain aminergic deficit in a genetic mouse model of phenylketonuria. *NeuroReport* 2000; **11**:1361–1364.
7 Pascucci T, Ventura R, Puglisi-Allegra S, Cabib S. Deficits in brain serotonin synthesis in a genetic mouse model of phenylketonuria. *NeuroReport* 2002; **13**:2561–2564.
8 Mochizuki S, Mizukami H, Ogura T, Kure S, Ichinohe A, Kojima K, *et al.* Long-term correction of hyperphenylalaninemia by AAV-mediated gene transfer leads to behavioral recovery in phenylketonuria mice. *Gene Ther* 2004; **11**:1081–1086.
9 Yagi H, Ogura T, Mizukami H, Urabe M, Hamada H, Yoshikawa H, *et al.* Complete restoration of phenylalanine oxidation in phenylketonuria mouse by a self-complementary adeno-associated virus vector. *J Gene Med* 2011; **13**:114–122.
10 Thöny B. Long-term correction of murine phenylketonuria by viral gene transfer: liver versus muscle. *J Inherit Metab Dis* 2010; **33**:677–680.
11 Kure S, Sato K, Fujii K, Aoki Y, Suzuki Y, Kato S, *et al.* Wild-type phenylalanine hydroxylase activity is enhanced by tetrahydrobiopterin supplementation in vivo: an implication for therapeutic basis of tetrahydrobiopterin-responsive phenylalanine hydroxylase deficiency. *Mol Genet Metab* 2004; **83**:150–156.
12 Sumi-Ichinose C, Urano F, Kuroda R, Ohye T, Kojima M, Tazawa M, *et al.* Catecholamines and serotonin are differently regulated by tetrahydrobiopterin: a study from 6-pyruvoyltetrahydropterin synthase knockout mice. *J Biol Chem* 2001; **276**:41150–41160.
13 Smith CB, Kang J. Cerebral protein synthesis in a genetic mouse model of phenylketonuria. *Proc Natl Acad Sci USA* 2000; **97**: 11014–11019.
14 Shulkin BL, Betz AL, Koeppe RA, Agranoff BW. Inhibition of neutral amino acid transport across the human blood-brain barrier by phenylalanine. *J Neurochem* 1995; **64**:1252–1257.

15 Pietz J, Kreis R, Rupp A, Mayatepek E, Rating D, Boesch C, *et al.* Large neutral amino acids block phenylalanine transport into brain tissue in patients with phenylketonuria. *J Clin Invest* 1999; **103**:1169–1178.
16 Curtius HC, Niederwiesser A, Viscontini M, Leimbacher W, Wagmann H, Blehova B, *et al.* Serotonin and dopamine synthesis in phenylketonuria. *Adv Exp Med Biol* 1981; **133**:277–291.
17 Ogawa S, Ichinose H. Effect of metals and phenylalanine on the activity of human tryptophan hydroxylase-2: comparison with that on tyrosine hydroxylase activity. *Neurosci Lett* 2006; **401**:261–265.
18 Joseph B, Dyer CA. Relationship between myelin production and dopamine synthesis in the PKU mouse brain. *J Neurochem* 2003; **86**:615–626.
19 Dyer CA, Kendler A, Philibotte T, Gardiner P, Cruz J, Levy HL. Evidence for central nervous system glial cell plasticity in phenylketonuria. *J Neuropath Exp Neur* 1996; **55**:795–814.
20 Embury JE, Charron CE, Martynyuk A, Zori AG, Liu B, Ali SF, *et al.* PKU is a reversible neurodegenerative process within the nigrostriatum that begins as early as 4 weeks of age in *Pah*^{enu2} mice. *Brain Res* 2007; **1127**:136–150.
21 Nathwani AC, Rosales C, McIntosh J, Riddel A, Rustagi P, Galder B, *et al.* Early clinical trial results following administration of a low dose of a novel self complementary adeno-associated viral vector encoding human factor ix in two subjects with severe haemophilia B. *Hum Gene Ther* 2010; **21**:1362.

THE JOURNAL OF GENE MEDICINE
J Gene Med 2011;**13**: 114–122.
Published online in Wiley Online Library (wileyonlinelibrary.com) **DOI**: 10.1002/jgm.1543

RESEARCH ARTICLE

Complete restoration of phenylalanine oxidation in phenylketonuria mouse by a self-complementary adeno-associated virus vector

Hiroya Yagi[1,2]
Tsuyoshi Ogura[2]
Hiroaki Mizukami[1]
Masashi Urabe[1]
Hiromi Hamada[2]
Hiroyuki Yoshikawa[2]
Keiya Ozawa[1]
Akihiro Kume[1]*

[1]*Division of Genetic Therapeutics, Center for Molecular Medicine, Jichi Medical University, Shimotsuke, Japan*

[2]*Department of Obstetrics and Gynecology, Institute of Clinical Medicine, University of Tsukuba, Tsukuba, Japan*

*Correspondence to: Akihiro Kume, Division of Genetic Therapeutics, Center for Molecular Medicine, Jichi Medical University, 3311-1 Yakushiji, Shimotsuke 329-0498, Japan
E-mail: kume@jichi.ac.jp

Received: 5 October 2010
Revised: 15 December 2010
Accepted: 24 January 2011

Abstract

Background Classical phenylketonuria (PKU) arises from a deficiency of phenylalanine hydroxylase (PAH) that catalyses phenylalanine oxidation in the liver. Lack of PAH activity causes massive hyperphenylalaninemia and consequently severe brain damage. Preclinical studies showed that conventional adeno-associated virus (AAV) vectors could correct hyperphenylalaninemia in a mouse model of PKU, although limitations such as very large dose requirement and relative inefficiency in female animals were recognized.

Method An AAV8-pseudotyped vector was constructed with a self-complementary AAV (scAAV) genome for efficient liver transduction and expression. Following vector injection to PKU mice, blood Phe was periodically measured by an enzymatic fluorometric assay. *In vivo* Phe oxidation was evaluated by a non-invasive breath test using [1-^{13}C]Phe. Vector copy number in the host tissues was determined by quantitative polymerase chain reaction.

Results A single injection of 1×10^{11}–1×10^{12} particles of the scAAV8 vector resulted in a reduction of blood Phe to normal or near-normal levels for more than 1 year in both genders. The treated animals showed normal level of *in vivo* Phe oxidation. The presence of >1 copy of vector DNA per diploid genome in the liver was associated with normal blood Phe in the AAV-treated PKU mice.

Conclusions Complete phenotypic correction of PKU mice was achieved by the scAAV8 vector for the longest duration reported to date. The vector overcame the female-specific disadvantage in AAV-mediated liver transduction; thus, it offers a promising platform of long-lasting gene therapy for PKU. Copyright © 2011 John Wiley & Sons, Ltd.

Keywords adeno-associated virus; gene therapy; phenylketonuria; phenylalanine oxidation

Introduction

Phenylketonuria (PKU; OMIM 261 600) is an autosomal recessive disorder caused by a deficiency of phenylalanine hydroxylase (PAH; EC 1.14.16.1) in the liver [1]. The enzyme is responsible for the major part of phenylalanine (Phe) clearance by converting Phe to tyrosine (Tyr) with the aid of tetrahydrobiopterin (BH_4) and molecular oxygen. Consequently, PAH deficiency leads to a massive accumulation of Phe under a normal

diet, which is toxic to the developing brain. Untreated patients are afflicted with severe mental retardation, seizure and growth failure, as well as hypopigmentation of the hair and skin. The current management for PKU mandates an early diagnosis by newborn screening followed by a Phe-restricted diet to prevent irreversible brain damage in infancy and childhood. Such a diet is also recommended for adult PKU patients to avoid problems associated with hyperphenylalaninemia, such as psychomotor dysfunction and teratogenic effects on fetuses carried by the female patients (so-called 'maternal PKU syndrome'). However, the unpalatable and expensive diet loads heavy burdens on the patients and their families. Therefore, an alternative approach to PKU, preferably achieving a life-long cure, is desired.

We and other investigators have explored the development of somatic gene therapy for PKU, which offers a novel therapeutic paradigm [2,3]. The most straightforward approach is to deliver the functional PAH gene to the liver, where the enzyme is normally expressed. In most preclinical studies, a mouse model of PKU (Pah^{enu2} strain developed in BTBR background) has been used because it shows a similar phenotype to human PKU [4,5]. Thus far, recombinant adeno-associated virus (AAV) vectors have shown the most promising results in correcting hyperphenylalaninemia in Pah^{enu2} mice [6–10]. Through these studies, however, two major problems were recognized. One was the relatively large dose requirement of AAV vectors to correct murine PKU phenotype compared to other disease models such as haemophilia B. The other problem was gender-dependent effectiveness of AAV vectors, particularly when they were targeted to the liver. That is, female Pah^{enu2} animals required greater AAV doses to reduce blood Phe, and the therapeutic effect was not long-lasting. This phenomenon was investigated in some detail with another animal model [11]. To enhance gene delivery and overcome these problems, attention has turned to alternative AAV serotypes with distinct tissue tropism (e.g. AAV8 for liver transduction) [12–14]. Pseudotyping with AAV8 capsid showed higher efficiency in treating Pah^{enu2} mice, together with *cis*-acting elements to enhance liver-specific transcription and mRNA transport [9,10].

In the quest for a further improvement in liver transduction, we realized that another drawback in AAV transduction should be circumvented. Because the single-stranded (ss) DNA genomes of conventional AAV vectors are transcriptionally inactive, they must become double-stranded (ds) to be expressed. The ss- to dsDNA conversion requires host cell-mediated DNA synthesis or annealing of complementary genomes from separate virions, which appears to be the rate-limiting step in AAV transduction [15,16]. This process can be bypassed with a self-complementary (sc) AAV vector because its genome DNA spontaneously self-anneals to form stable dsDNA in the host cell [17–19]. Therefore, we investigated the efficacy of a self-complementary AAV (scAAV) vector for the treatment of Pah^{enu2} mice.

Materials and methods

Vector construction

A serotype 8-pseudotyped ssAAV vector for PKU (ssAAV8/CAG-mPAH) was constructed with ssAAV/CAG-mPAH plasmid (Figure 1, top) used in our previous study [7,20]. A scAAV8 vector was constructed with scAAV/LP1-hFIX plasmid carrying the human factor IX (hFIX) gene (kindly provided by Dr John T. Gray, St Jude Research Hospital, Memphis, TN, USA) [21]. For vector-derived PAH expression, the hFIX sequence (*Eco*R I-*Xho* I) in scAAV/LP1-hFIX was replaced with the murine PAH (mPAH) cDNA (*Eco*R I-*Sal* I) from ssAAV/CAG-mPAH (Figure 1, bottom). AAV8-pseudotyoed vector stocks were propagated by an adenovirus-free, three-plasmid transfection method [22]. Briefly, a 10-tray Cell Factory container (CF10; Nalge Nunc International, Rochester, NY, USA) of semiconfluent 293 cells were cotransfected with 650 μg of AAV/CAG-mPAH or scAAV/LP1-mPAH plasmid, 650 μg of AAV2 rep-AAV8 cap helper plasmid (pRep-Cap8 from Dr J. M. Wilson [12]) and 650 μg of adenoviral helper plasmid (pAdeno [23]) by standard calcium phosphate method. Cells were incubated with active gassing for 3 days and harvested [24]. AAV vectors were purified from the crude cell extract by serial ultracentrifugation with CsCl. Vector genome (vg) titers were determined by dot blot hybridization with the mPAH cDNA probe [7]. For scAAV8/LP1-mPAH, titration was also carried out by quantitative polymerase chain reaction (qPCR), where scAAV8/LP1-mPAH and the vector plasmid standard were amplified with a primer set (5′-ACAGTGAATCCGGACTCTAAGG-3′ and 5′-CTGCTCAGGACTCCGTTCTC-3′) using a real-time PCR instrument (7900HT; Applied Biosystems, Foster City, CA, USA). A 136-bp region between LP1 promoter and the mPAH cDNA was amplified and confirmed by agarose gel electrophoresis. The qPCR-based titer was calibrated with the result of other titration methods described previously [25,26].

Animals and gene delivery

Colonies of a PKU model mouse, BTBR-Pah^{enu2} and its wild-type (WT) strain BTBR (obtained from Jackson Laboratories, Bar Harbor, ME, USA) were maintained in the animal facility of Jichi Medical University. All animals were fed standard mouse chow (CE-2 from Clea Japan, Tokyo, Japan) *ad libitum* providing approximately 25% of energy as protein. Genotyping for the presence of the Pah^{enu2} mutation was performed by PCR analysis of tail biopsy DNA. In brief, exon 7 (136 bp) of the mPAH gene was amplified with a primer set (5′-CTTGTACTGGTTTCCGCCTC-3′ and 5′-GG TTCAGGTGTGTACATGGG-3′). The amplified DNA from WT allele is cleaved by *Mbo*II into 70-bp and 66-bp fragments, whereas the counterpart from Pah^{enu2} allele is uncleavable as a result of the c.835T → C (F263S) mutation [5]. The scAAV vector (1×10^{11} to 3×10^{12}

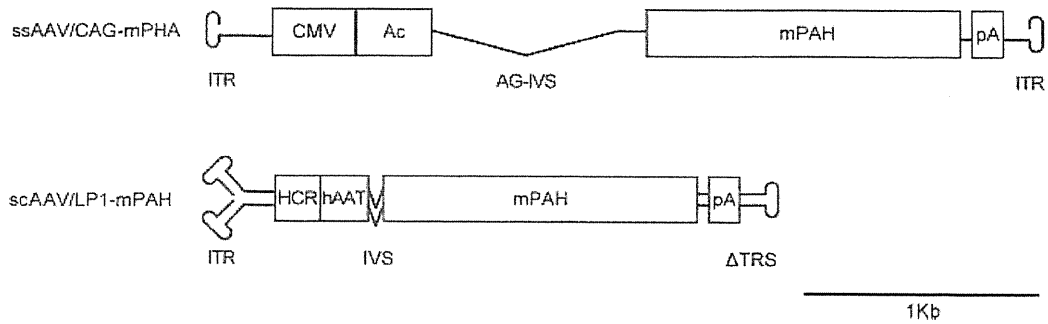

Figure 1. Structure of AAV vectors for PKU gene therapy. Top: ssAAV/CAG-mPAH vector. CAG promoter consists of the human cytomegalovirus immediate-early enhancer (CMV), the chicken β-actin promoter (Ac) and a chicken β-actin/rabbit β-globin composite intron (AG-IVS). CAG promoter, the murine phenylalanine hydroxylase cDNA (mPAH) and the SV40 late polyadenylation signal (pA) are flanked by the AAV inverted terminal repeats (ITR). Bottom: scAAV/LP1-mPAH vector. LP1 promoter consists of the human apolipoprotein E/C-I hepatic control region (HCR) and the human α1-antitrypsin promoter (hAAT). In addition, the vector contains a modified SV40 small t-antigen intron (IVS), mPAH and pA. The entire expression cassette is flanked by the intact AAV ITR and the terminal resolution site-deleted ITR (ΔTRS)

particles) was dissolved in 0.5 ml of saline and injected into the peritoneal cavity of *Pah*^{enu2} mice. All animal experiments were carried out in accordance with the institutional guidelines under protocols approved by the Institutional Animal Care and Use Committee at Jichi Medical University.

Blood Phe assay

Blood Phe was measured by an enzymatic fluorometric assay using an Enzaplate PKU-R kit (GE Healthcare, Tokyo, Japan) [7]. Mice were tail phlebotomized and 30–40 μl of blood was spotted onto a paper filter (No. 545 for newborn mass screening; Advantec Toyo, Tokyo, Japan). A disc (3 mm in diameter) was punched out from the dried blood spot and placed in a round-bottom, 96-well microtiter plate. Phe was eluted from the disc and incubated with resazurin and Phe dehydrogenase, an NAD-dependent enzyme. The enzyme reaction produces NADH, which in turn converts resazurin to resorufin with the aid of diaphorase. The resultant resorufin was measured on a Fluoroskan Ascent plate reader (Labsystems, Helsinki, Finland) with a 544 nm/590 nm filter set.

Evaluation of *in vivo* Phe oxidation

In vivo Phe oxidation activity was evaluated by a method of Kure *et al.* [27] with slight modification. [1-^{13}C]L-Phe (^{13}C-Phe; from Cambridge Isotope Laboratories, Andover, MA, USA) and L-Phe (from Wako Pure Chemicals, Osaka, Japan) were dissolved in saline at 200 mg/ml and 20 mg/ml, respectively, and sterilized through 0.22-μm syringe filters (Millex-GV, Millipore, Yonezawa, Japan) immediately before intraperitoneal (i.p.) injection. Mice were preloaded with 20 mg/kg of L-Phe 30 min prior to ^{13}C-Phe challenge (2 mg/kg). Each mouse was kept in a lid-sealable plastic box for 15 min before and 45 min after ^{13}C-Phe challenge, and a total volume of 120 ml of air was transferred to a sampling bag for [^{13}C]urea breath test (Otsuka Pharmaceuticals, Tokyo, Japan) with a glass syringe. The ratio of $^{13}CO_2$ and $^{12}CO_2$ was measured by gas chromatography-mass spectrometry (GC-MS; by SRL, Tokyo, Japan), and the difference was designated as $\Delta^{13}CO_2$.

Determination of vector biodistribution

Tissue genomic DNA was extracted by a standard method using proteinase K (Boehringer Manheim, Manheim, Germany) and phenol:chloroform (Nippon Gene, Toyama, Japan). To quantify genomic DNA copy number, a unique region of the murine β-actin gene was amplified by qPCR with a primer set (5′-GGTCCTGG ATCACTCAGAACGGACACCA-3′ and 5′-AGCCTCAATAC GCACGCGCAGCTAAC-3′) along with a plasmid control. Vector copy number in tissue DNA was estimated by qPCR in the same manner as in vector titration.

Statistical analysis

Statistical analysis was performed using StatView, version 5.0, for Macintosh (SAS Institute, Cary, NC, USA). A paired *t*-test and unpaired *t*-test (Student's *t*-test or Welch's *t*-test) were used for comparison between the two groups. $p < 0.05$ was considered statistically significant for all analyses.

Results

Construction of AAV8 vectors for PKU

For comparison with scAAV8, a reference ssAAV8 vector was constructed with ssAAV/CAG-mPAH plasmid (Figure 1, top) [7]. Although the CAG promoter allowed very high hepatic expression in our previous studies

with ssAAV2 and ssAAV5 [7,28], the size of CAG-mPAH expression cassette (3.5 kb) exceeded the limit of packaging capacity of a scAAV vector (up to 2.2 kb). To meet the packaging requirements of scAAV, Nathwani *et al.* [21] developed a compact hFIX expression cassette (LP1-hFIX; 2.1 kb) and assembled it in the modified AAV2 backbone with an intact 5′ terminal resolution site (*trs*) and a deleted 3′ *trs* (scAAV/LP1-hFIX). The LP1 hybrid enhancer/promoter consists of the core liver-specific elements from the human apolipoprotein E/C-I gene hepatic control region (HCR) and the human α1-antitrypsin promoter (hAAT). The expression cassette also contains a modified SV40 small t-antigen intron and the SV40 late polyadenylation signal. Because the coding sequences of mPAH (1362 bp) and hFIX (1386 bp) have almost identical lengths, we constructed scAAV/LP1-mPAH vector by replacing the hFIX cDNA in scAAV/LP1-hFIX with the mPAH cDNA from ssAAV/CAG-mPAH (Figure 1, bottom). PAH expression from the resultant plasmid (scAAV/LP1-mPAH) was confirmed by transfection of Huh7 cells and immunoblotting (data not shown). The ssAAV/CAG-mPAH and scAAV/LP1-mPAH genomes were packaged into AAV serotype 8 capsid and titrated by dot blot hybridization. The determined titers of viral stocks were approximately 1×10^{13} vg/ml for ssAAV8/CAG-mPAH and 6×10^{13} vg/ml for scAAV8/LP1-mPAH, respectively. scAAV8/LP1-mPAH was also titrated by qPCR along with a plasmid control and calibrated with the result obtained from dot blot hybridization [25].

Efficacy of ssAAV8 in PKU mice

We previously reported that 1×10^{13} vg of ssAAV5/CAG-mPAH partially corrected hyperphenylalaninemia in male *Pah*^{enu2} mice when administered through the portal vein (PV) [7]. Meanwhile, ssAAV8 vectors delivered reporter genes to adult mouse liver with comparable efficiency following either i.p. or intravenous injection, with an apparent gender-specific barrier [29,30]. Therefore, we administered a log-smaller dose (1×10^{12} vg) of ssAAV8/CAG-mPAH vector to the peritoneal cavity of male PKU mice. This procedure resulted in an almost complete correction of hyperphenylalaninemia for 24 weeks (Figure 2a), confirming a very efficient liver transduction by AAV8. This observation prompted us to carry out a similar comparative study with female *Pah*^{enu2}. When female PKU mice were given 1×10^{13} vg of ssAAV8/CAG-mPAH through PV, blood Phe was rapidly decreased to normal levels (<2 mg/dl), and the initial impact on blood Phe was identical to that of PV-injected 1×10^{14} vg of ssAAV5/CAG-mPAH (Figure 2b). The therapeutic effect was transient, however, and hyperphenylalaninemia gradually resumed to the pretreatment level by 24 weeks post-injection. The same dose (1×10^{13} vg) of i.p.-injected ssAAV8/CAG-mPAH exhibited minimal effect on blood Phe during the observation period (Figure 2b). Taken together, the liver transduction efficiency of the ssAAV8 vector was

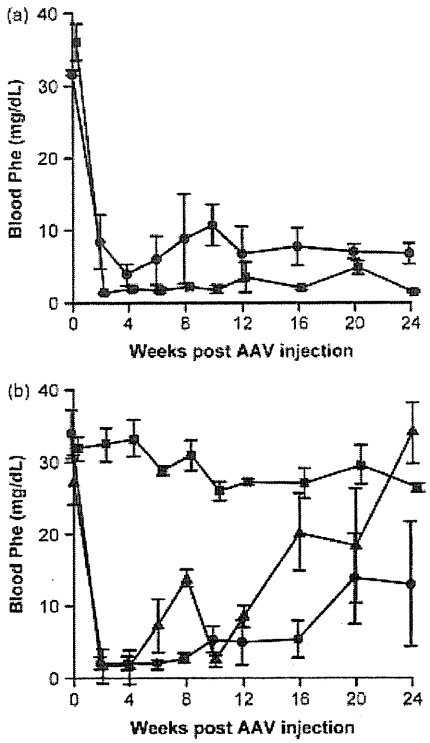

Figure 2. Efficacy of ssAAV5 and ssAAV8 vectors in *Pah*^{enu2} mice. (a) Male *Pah*^{enu2} mice were given either 1×10^{13} vg of ssAAV5/CAG-mPAH through the portal vein (PV) (circles, $n = 4$; data adopted from Mochizuki *et al.* [7]), or 1×10^{12} vg of ssAAV8/CAG-mPAH by i.p. (squares, $n = 3$). Blood Phe (mg/dl) levels are shown as the mean ± SD. (b) Female *Pah*^{enu2} mice were given either 1×10^{14} vg of ssAAV5/CAG-mPAH via the PV (circles, $n = 5$; data adopted from Mochizuki *et al.* [7]), 1×10^{13} vg of ssAAV8/CAG-mPAH via the PV (triangles, $n = 4$), or 1×10^{13} vg of ssAAV8/CAG-mPAH by i.p. injection (squares, $n = 3$). Blood Phe (mg/dl) levels are shown as the mean ± SD

greater than that of ssAAV5 by tenfold, although the gender-specific barrier was not overcome. Regarding the administration route of AAV8, PV injection was superior to i.p. injection, although the latter procedure was useful in male mice.

Short-term efficacy of scAAV8 in Phe metabolism of female PKU mice

Based on the above result with the ssAAV8 vector, we realized that further improvement was required to cure female *Pah*^{enu2} mice. Therefore, we addressed whether the self-complementary AAV genome would boost liver transduction. We gave 1×10^{11} or 1×10^{12} vg of scAAV8/LP1-mPAH to the peritoneal cavity of adult female *Pah*^{enu2} (8 weeks of age). These doses were two to three logs smaller than those of ssAAV5 and ssAAV8 vectors showing a transient therapeutic effect on female *Pah*^{enu2} (Figure 2b). When fed standard chow, the blood Phe concentration in WT BTBR mice was below 1.7 mg/dl (100 μM), whereas that in untreated *Pah*^{enu2} mice was above 20 mg/dl (1200 μM) (Table 1).

DOI: 10.1002/jgm

Table 1. Blood Phe, *in vivo* Phe oxidation and liver vector DNA in female *Pah*^{enu2} mice after 8 weeks of scAAV8/LP1-mPAH injection

Genotype/dose (vg)	Phe (mg/dl)	$\Delta^{13}CO_2$ (‰)	Vector DNA (c/dg)
WT/none ($n = 7$)	0.7 ± 0.1	38.9 ± 14.8	ND
Pah^{enu2}/none ($n = 8$)	32.5 ± 6.2	1.1 ± 0.8	ND
Pah^{enu2}/1 × 10^{11} ($n = 4$)	1.8 ± 0.5	32.8 ± 13.4	1.5 ± 0.3
Pah^{enu2}/1 × 10^{12} ($n = 4$)	1.0 ± 0.3	39.5 ± 13.0	27.3 ± 16.0

ND, not determined.

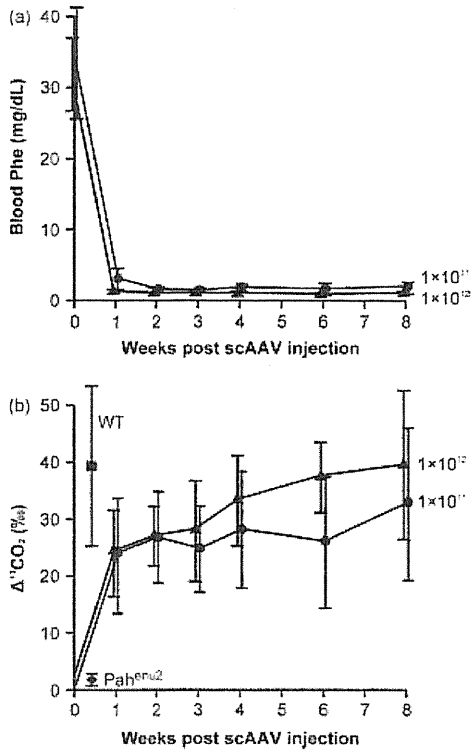

Figure 3. Short-term efficacy of scAAV8/LP1-mPAH in female *Pah*^{enu2} mice after i.p. injection. (a) Weekly blood Phe (mg/dl) levels are depicted as the mean ± SD. (b) *In vivo* Phe oxidation ($\Delta^{13}CO_2$‰) levels are represented as the mean ± SD of each dosage group. Circles, BTBR-*Pah*^{enu2} given 1 × 10^{11} vg of scAAV8 ($n = 4$); triangles, BTBR-*Pah*^{enu2} given 1 × 10^{12} vg ($n = 4$); square, wild-type BTBR (WT, $n = 7$); diamond, untreated BTBR-*Pah*^{enu2} (Pah^{enu2}, $n = 8$)

Following a single i.p. injection of scAAV8/LP1-mPAH, a dramatic decrease of blood Phe was observed in female *Pah*^{enu2} (Figure 3a). In mice receiving 1 × 10^{11} vg of vector, blood Phe was decreased from 33.3 ± 7.8 mg/dl to 3.0 ± 1.5 mg/dl ($n = 4$; $p < 0.01$) in 1 week and kept within the normal range 2–8 weeks post-injection (Table 1). In mice receiving 1 × 10^{12} vg of vector, hyperphenylalaninemia was corrected even more rapidly and uniformly; blood Phe was normalized in 1 week (from 31.7 ± 5.1 to 1.2 ± 0.3 mg/dl, $n = 4$; $p < 0.01$) through 8 weeks after treatment (Table 1). Between these two dosage groups, the blood Phe concentration was not significantly different, except for the data obtained 2 weeks post-i.p. ($p < 0.05$). With normalization of blood Phe, hypopigmentation in the treated mice was gradually ameliorated. Patchy black hair emerged by week 2, and the animals recovered the WT coat color by week 8.

In parallel with blood Phe analysis, we evaluated the *in vivo* oxidation capacity for Phe by a non-invasive breath test. In this assay, administered ^{13}C-Phe is converted to [1-^{13}C]Tyr by PAH, which is then broken down to yield homogentisic acid and $^{13}CO_2$ by two enzymatic reactions. Eventually, $^{13}CO_2$ is liberated into breath, and the $^{13}CO_2$ concentration (as a ratio to $^{12}CO_2$) is measured by infrared spectrophotometry or GC-MS. Because our initial experiments showed that GC-MS offered lower background, this method was used in the subsequent investigation. The amount of $^{13}CO_2$ production ($\Delta^{13}CO_2$) is determined by the difference between the $^{13}CO_2$ concentration of the breath samples collected before and after ^{13}C-Phe infusion. Because a significant fraction of input ^{13}C-Phe is metabolized through the above pathway where PAH catalyses the rate-limiting step, we can evaluate PAH activity by measuring $\Delta^{13}CO_2$ [27]. WT mice showed positive $\Delta^{13}CO_2$ values without an apparent gender difference (males: 45.5 ± 8.8‰, $n = 7$; females: 38.9 ± 14.8‰, $n = 7$). By contrast, untreated *Pah*^{enu2} mice produced very little, if any, $\Delta^{13}CO_2$ in the breath test (males: 1.0 ± 0.6‰, $n = 3$; females: 1.1 ± 0.8‰, $n = 8$), resulting from the absence of PAH activity (Table 1). The impaired *in vivo* Phe oxidation was rapidly corrected following scAAV8/LP1-mPAH injection, in a reciprocal fashion to blood Phe reduction (Figure 3b). In the female *Pah*^{enu2} mice receiving 1 × 10^{11} vg of vector, $\Delta^{13}CO_2$ was improved from 0.9 ± 0.8‰ to 23.6 ± 10.2‰ in 1 week ($n = 4$; $P < 0.05$) and maintained in a near-normal to normal range thereafter. In mice receiving 1 × 10^{12} vg of vector, $\Delta^{13}CO_2$ was increased from 1.4 ± 0.9‰ to 24.2 ± 7.5‰ at week 1 ($n = 4$; $p < 0.01$) with an upward tendency until week 8 (Table 1).

After 8 weeks post-i.p., the animals were euthanized for tissue DNA analysis for vector biodistribution. The vector content in the liver was 1.5 ± 0.3 and 27.3 ± 16.0 copies/diploid genome (c/dg) in the low- (1 × 10^{11} vg, $n = 4$) and high-dosage (1 × 10^{12} vg, $n = 4$) groups, respectively ($p < 0.05$; Table 1). Although the vector DNA was barely detected (<0.01 c/dg) in the spleen and gonads from mice given 1 × 10^{12} vg of vector, a trace amount of vector (0.3–0.5 c/dg) was present in these viscera from the mice receiving 1 × 10^{12} vg. The DNA analysis recapitulated a very strong liver tropism of scAAV8 vectors as reported previously [21].

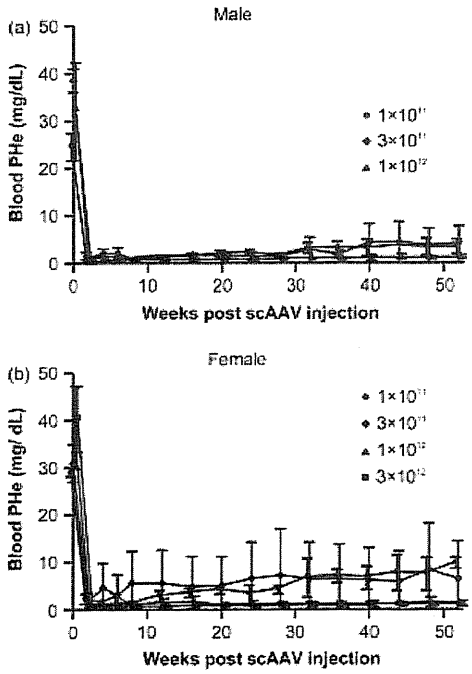

Figure 4. Long-term efficacy of i.p.-injected scAAV8/LP1-mPAH in *Pah*^{enu2} mice. (a) Male *Pah*^{enu2} mice were administered either 1×10^{11} vg (circles, $n = 4$), 3×10^{11} vg (diamonds, $n = 3$) or 1×10^{12} vg (triangles, $n = 3$) of scAAV8/LP1-mPAH, and the data are depicted as the mean ± SD blood Phe (mg/dl) versus weeks post-injection of scAAV8. (b) Female *Pah*^{enu2} mice were given either 1×10^{11} vg (circles, $n = 3$), 3×10^{11} vg (diamonds, $n = 3$), 1×10^{12} vg (triangles, $n = 4$) or 3×10^{12} vg (squares, $n = 4$) of scAAV8/LP1-mPAH, and the data are shown as the mean ± SD blood Phe (mg/dl)

Long-term correction of hyperphenylalaninemia in both genders

Encouraged by the shot-term efficacy of scAAV8/LP1-mPAH vector in female *Pah*^{enu2}, we treated several cohorts of PKU mice with the same vector for longer observation ($n = 3$–4 each). Male and female *Pah*^{enu2} mice (6–8 weeks of age) were given either 1×10^{11}, 3×10^{11} or 1×10^{12} vg of scAAV8/LP1-mPAH by i.p. injection. An additional female cohort was given a higher dose (3×10^{12} vg), in consideration of the possibility of temporary transgene expression in this gender. The treated mice were phlebotomized for blood Phe analysis every 2–4 weeks, and Figure 4 shows the kinetics of blood Phe concentration for 1 year following vector administration. In males, Phe levels decreased to normal with all doses (1×10^{11} vg, from 25.1 ± 2.3 to 1.1 ± 0.3 mg/dl; 3×10^{11} vg, from 38.3 ± 2.7 to 0.8 ± 0.6 mg/dl; 1×10^{12} vg, from 32.5 ± 9.7 to 0.4 ± 0.1 mg/dl) at week 2 (Figure 4a). All males with 1×10^{12} vg ($n = 3$) and two out of three males with 3×10^{11} vg maintained normal blood Phe (<1.7 mg/dl) throughout 1-year observation, whereas one with 3×10^{11} vg showed a mild elevation (8–9 mg/dl) from 32 weeks post-i.p. One male with 1×10^{11} vg upheld normal blood Phe, whereas three out of four in this cohort had slightly increased blood Phe from 32 weeks that was within the therapeutic range (2–6 mg/dl). A similar, although slightly limited long-term efficacy was observed in females (Figure 4b). In the female *Pah*^{enu2} mice with 3×10^{12} vg ($n = 4$) or 1×10^{12} vg ($n = 4$) of vector, blood Phe decreased to normal in 2 weeks (from 40.2 ± 7.0 to 0.7 ± 0.4 mg/dl, and 38.5 ± 8.7 to 0.6 ± 0.2 mg/dl, respectively) and maintained that level for 1 year. In females with 3×10^{11} vg, two out of three animals sustained normal blood Phe, whereas the other mouse lost control after 4 weeks with moderate hyperphenylalaninemia (10–15 mg/dl). In females with 1×10^{11} vg ($n = 3$), blood Phe was corrected initially (from 29.1 ± 1.0 to 1.5 ± 0.5 mg/dl at week 4), although the level was gradually increased to near-normal (2–6 mg/dl at weeks 12–28) and then mild hyperphenylalaninemic range (6–10 mg/dl at weeks 32–52). Despite such variability being observed in a limited number of animals, the reduction of blood Phe was significant in all the cohorts throughout the observation period. This result clearly demonstrated the superb efficacy of scAAV8/LP1-mPAH vector in treating murine PKU. We assumed that the vector threshold dose

Table 2. Remote phase blood Phe, *in vivo* Phe oxidation and vector DNA in the liver

Gender	Dose (vg)	Phe (mg/dl)	$\Delta^{13}CO_2$ (‰)	Vector DNA (c/dg)
Male	1×10^{11}	3.9	18.31	0.88
	1×10^{11}	3.0	32.54	0.57
	3×10^{11}	1.7	52.18	1.34
	3×10^{11}	2.1	19.54	1.16
	1×10^{12}	3.3	45.34	9.95
	1×10^{12}	1.2	ND	7.85
Female	1×10^{11}	12.4	3.96	0.17
	1×10^{11}	8.9	1.57	0.22
	3×10^{11}	4.2	5.62	0.48
	1×10^{12}	1.6	60.44	3.13
	3×10^{12}	1.3	23.31	6.38
	3×10^{12}	2.4	62.95	6.47
	3×10^{12}	1.2	55.60	9.26

ND, not determined.

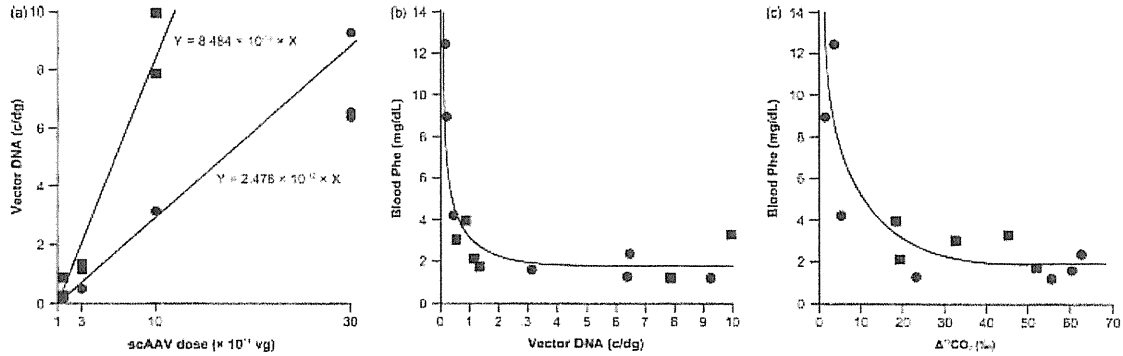

Figure 5. Relationships among vector dose, blood Phe, *in vivo* Phe oxidation and vector DNA content in remote phase. (a) Relationship between the given dose of scAAV8/LP1-mPAH (vg; *x*-axis) and vector DNA content in the liver (c/dg; *y*-axis). Plots with males (squares) fit a regression line of $y = 8.484 \times 10^{-12}x$, whereas plots with females (circles) fit a line of $y = 2.478 \times 10^{-12}x$. (b) Relationship between the vector DNA in the liver (c/dg; *x*-axis) and blood Phe (mg/dl; *y*-axis). Males (squares) and females (circles) fit a single hyperbolic-like curve. (c) Relationship between *in vivo* Phe oxidation ($\Delta^{13}CO_2$‰; *x*-axis) and blood Phe (mg/dl; *y*-axis). Plots of males (squares) and females (circles) fit a single hyperbolic-like curve

to correct hyperphenylalaninemia was 1×10^{11} vg or less for male Pah^{enu2} mice, and slightly over 1×10^{11} vg for females that would be a half-log higher. A gender-specific difference appears to exist with scAAV8 as well, although the barrier in female animals may be smaller than that with ssAAV vectors.

Correlation between transduction rate and function in remote phase

After confirming the long-term efficacy of the scAAV8 vector in both genders, we examined *in vivo* Phe oxidation and tissue DNA in several *Pah*^{enu2} mice later than 1 year after scAAV8 injection. Table 2 summarizes the data obtained for six males and seven females evaluated at 60–80 weeks post-i.p., and Figure 5 shows the relationships among the parameters chosen. The amount of vector DNA in the liver showed a linear relationship with the given vector dose, and was not saturated within the dose range used in the present study (Figure 5a). Compared with the data for 8 weeks post-i.p. (Table 1), the vector DNA content in the treated females was approximately one-tenth in the remote phase, suggesting a slow but substantial vector loss. The lines best fit the data were $y = 8.484 \times 10^{-12}x$ ($r^2 = 0.962, p < 0.0001$) for males and $y = 2.478 \times 10^{-12}x$ ($r^2 = 0.967, p < 0.0001$) for females, respectively (x, vector dose in vg; y, vector DNA in the liver in c/dg). Thus, male livers were more efficiently transduced than female livers by 3.4-fold, in agreement with the above assumption of vector doses for correcting hyperphenylalaninemia in these genders.

Once the liver was transduced, the vector appeared to impact on Phe metabolism in the same, or nearly identical mode in both genders. Figure 5b shows the relationship between liver vector copy number and blood Phe. Plots for male (squares) and female (circles) livers appear to fit into quite analogous, if not identical, hyperbolic-like curves. Blood Phe levels were steeply reduced to normal as the vector copy number increased from 0 to 1 c/dg, and no further reduction was observed with more vector DNA in the liver. Therefore, Phe was normalized by the presence of 1 or more vector c/dg, regardless of gender. The result suggests that the larger dose requirement of scAAV8 to correct female hyperphenylalaninemia resulted not from poorer transgene expression but from a lower transduction efficiency. Figure 5c shows the relationship between *in vivo* Phe oxidation and blood Phe. Again, plots of both males (squares) and females (circles) appear to fit an almost identical hyperbolic-like curve. Earlier preclinical studies showed that recovery of 10–20% of normal PAH activity was sufficient to normalize blood Phe in *Pah*^{enu2} mice, in agreement with accumulated clinical data [1,9,31]. Because we observed a significant baseline deviation and fluctuation of $\Delta^{13}CO_2$ in WT animals (Table 1) partly because of the relative BH_4 insufficiency *in vivo* [27], it was difficult to calculate the actual recovery of Phe oxidation capacity of the treated *Pah*^{enu2} mice. Nevertheless, it is noteworthy that some animals showed physiological or even higher levels of Phe catabolism, even for extended periods (60–80 weeks) after scAAV8 injection.

Discussion

In the present study, we showed a long-term efficacy of a scAAV8 vector for murine PKU in both genders. To our knowledge, the vector allowed the longest duration (up to 80 weeks) of correcting hyperphenylalaninemia, particularly in female *Pah*^{enu2}, by gene transfer. We previously showed successful correction of hyperphenylalaninemia in *Pah*^{enu2} mice with a ssAAV5 vector, although the effect was partial and transient in females [7]. Type 8-pseudotyping of that vector increased the initial efficacy by more than ten-fold, although the therapeutic benefit waned over time in female *Pah*^{enu2}. Other studies also recognized a similar female disadvantage with ssAAV8, although it was

DOI: 10.1002/jgm

milder than that with ssAAV2 and ssAAV5 [14,32]. On the other hand, Ding *et al.* [10] normalized blood Phe in both male and female *Pah*^{enu2} mice with a ssAAV8 vector up to 42 weeks. Following an injection of relatively large dose (5×10^{12} vg) of ssAAV8, they found very high copy number (>1000 c/dg) of vector DNA in the liver of their animals, which was 20–50-fold greater than than that in other studies including our own. If this was indeed the case, such an excess amount of vector, at least in part, may account for the adequate PAH expression that would overcome the female disadvantage.

In our experimental setting, the scAAV genome structure finally allowed a robust and stable liver transduction in female mice. In accordance with our results, recent studies have demonstrated the advantage of scAAV vectors in liver-directed gene transfer, particularly in combination with the serotype 8 capsid [32–35]. Pañeda *et al.* [32] extensively studied the efficiency of pseudotyped ssAAV and scAAV vectors and showed a significant advantage of scAAV8 in female mice. Furthermore, using the same vector platform (scAAV8/LP1) as in the present study, Vaessen *et al.* [33] showed a near-physiological transgene expression in a murine apolipoprotein A-I deficiency model, whereas Wu *et al.* [34] suggested that further fine-tuning of the vector should increase the efficacy. Because the therapeutic end point for PKU gene transfer is relatively high (>10% of normal PAH activity), these investigations are quite encouraging. Interestingly, Nathwani *et al.* [35] observed that preadministration of bortezomib, a proteasome inhibitor, augmented liver transduction with a scAAV8 vector in female mice by two-fold, whereas the enhancement in male animals was more modest. A detailed understanding of the molecular events in AAV transduction should allow such pharmacological support for better gene transfer in actual clinical settings.

One of the issues addressed in the present study was how many AAV vector copies in the liver would be required for persistent phenotypic correction of PKU. In the analysis at 8 weeks post-i.p., we found 1.5 ± 0.3 c/dg following 1×10^{11} vg i.p. and 27.3 ± 16.0 c/dg following 1×10^{12} vg i.p. (Table 1), whereas other studies detected more AAV genomes in their mouse liver. For example, Harding *et al.* [9] detected 16–51 c/dg of vector DNA in the mouse liver 8–17 weeks after they injected 5×10^{11} vg of ssAAV8, and Nakai *et al.* [36] found 58.2 ± 10.9 c/dg of vector 6 weeks after 3×10^{11} vg of ssAAV8. Presumably, our method of AAV administration (i.p.) was relatively less efficient compared to the PV injection that these investigators carried out. However, the reason for the large discrepancy compared to another study [10] (>1000 c/dg) is unknown. After initial transduction of the liver, the recombinant AAV genomes may be gradually degraded or diluted because they are present as episomes [37]. Indeed, we observed that the vector DNA was decreased to one-tenth in the animal liver after 1 year. At this stage, we demonstrated that the threshold of the therapeutic vector DNA in the tissue was approximately 1 c/dg. To extend gene transfer efficacy, a new strategy may be required. Integrating vectors are maintained if they do not elicit immunological responses, although most of them have some genotoxicity at the expense of stability through mitosis. Site-specific integrases may offer safer and stable transduction [38], although the delivery vehicle for such a strategy is currently underdeveloped. Alternatively, targeting extrahepatic tissues for PKU gene therapy has been discussed. In particular, skeletal muscle is an attractive target because of its slow turnover and easy accessibility [3,39,40]. One of the problems with this approach is how to deliver cofactor BH_4 to the exogenously expressed PAH in a clinically feasible way.

In summary, a single injection of scAAV8 vector corrected hyperphenylalaninemia in male and female PKU mice for the longest period reported to date. Although it is difficult to translate murine experiments into human PKU directly, the accumulating safety and efficacy studies of AAV gene transfer to larger animals are very informative. Together with an encouraging result obtained in a haemophilia B clinical trial started recently [41], these investigations will help to develop a safe and long-lasting gene transfer strategy for PKU treatment.

Acknowledgements

The authors are grateful to Takashi Matsushita and Miyoko Mitsu for vector preparation, as well as Kiyomi Aoki for the manuscript artwork. This work was supported in part by Grants-in-Aid for Scientific Research from the Ministry of Education, Culture, Sports, Science and Technology-Japan (#20591230). The authors have no relevant conflicts of interest to declare.

References

1. Scriver CR, Kaufman S. Hyperphenylalaninemia: phenylalanine hydroxylase deficiency. In The Metabolic and Molecular Bases of Inherited Disease, Scriver CR, Beaudet AL, Sly WS, Valle D (eds). McGraw-Hill: New York, NY, 2001; 1667–1724.
2. Eisensmith RC, Woo SLC. Gene therapy for phenylketonuria. *Eur J Pediatr* 1996; **155**: S16–S19.
3. Thöny B. Long-term correction of murine phenylketonuria by viral gene transfer: liver versus muscle. *J Inherit Metab Dis* 2010; **33**: 677–680.
4. Shedlovsky A, McDonald JD, Symula D, Dove WF. Mouse models of human phenylketonuria. *Genetics* 1993; **134**: 1205–1210.
5. McDonald JD, Charlton CK. Characterization of mutations at the mouse phenylalanine hydroxylase locus. *Genomics* 1997; **39**: 402–405.
6. Laipis PJ, Charron C, Ross K, *et al.* Long-term correction of phenylketonuria in an animal model by recombinant AAV-based gene therapy. *J Inherit Metab Dis* 2002; **25**: 615–616.
7. Mochizuki S, Mizukami H, Ogura T, *et al.* Long-term correction of hyperphenylalaninemia by AAV-mediated gene transfer leads to behavioral recovery in phenylketonuria mice. *Gene Ther* 2004; **11**: 1081–1086.
8. Oh H, Park E, Kang S, Jo I, Jung S. Long-term enzymatic and phenotypic correction in the phenylketonuria

mouse model by adeno-associated virus vector-mediated gene transfer. *Pediatr Res* 2004; **56**: 278–284.
9. Harding CO, Gillingham MB, Hamman K, *et al.* Complete correction of hyperphenylalaninemia following liver-directed, recombinant AAV2/8 vector-mediated gene therapy in murine phenylketonuria. *Gene Ther* 2006; **13**: 457–462.
10. Ding Z, Georgiev P, Thöny B. Administration-route and gender-independent long-term therapeutic correction of phenylketonuria (PKU) in a mouse model by recombinant adeno-associated virus 8 pseudotyped vector-mediated gene transfer. *Gene Ther* 2006; **13**: 587–593.
11. Davidoff AM, Ng CYC, Zhou J, Spence Y, Nathwani AC. Sex significantly influences transduction of murine liver by recombinant adeno-associated viral vectors through an androgen-dependent pathway. *Blood* 2003; **102**: 480–488.
12. Gao GP, Alvira MR, Wang L, Calcedo R, Johnston J, Wilson JM. Novel adeno-associated viruses from rhesus monkeys as vectors for human gene therapy. *Proc Natl Acad Sci USA* 2002; **99**: 11854–11859.
13. Davidoff AM, Gray JT, Ng CYC, *et al.* Comparison of the ability of adeno-associated viral vectors pseudotyped with serotype 2, 5 and 8 capsid proteins to mediate efficient transduction of the liver in murine and nonhuman primate models. *Mol Ther* 2005; **11**: 875–888.
14. Wang L, Calcedo R, Nichols TC, *et al.* Sustained correction of disease in naive and AAV2-pretreated hemophilia B dogs: AAV2/8-mediated, liver-directed gene therapy. *Blood* 2005; **105**: 3079–3086.
15. Russell DW, Kay MA. Adeno-associated virus vectors and hematology. *Blood* 1999; **94**: 864–874.
16. Nakai H, Storm TA, Kay MA. Recruitment of single-stranded recombinant adeno-associated virus vector genomes and intermolecular recombination are responsible for stable transduction of liver in vivo. *J Virol* 2000; **74**: 9451–9463.
17. McCarty DM, Monahan PE, Samulski RJ. Self-complementary recombinant adeno-associated virus (scAAV) vectors promote efficient transduction independently of DNA synthesis. *Gene Ther* 2001; **8**: 1248–1254.
18. McCarty DM, Fu H, Monahan PE, Toulson CE, Naik P, Samulski RJ. Adeno-associated virus terminal repeat (TR) mutant generates self-complementary vectors to overcome the rate-limiting step to transduction in vivo. *Gene Ther* 2003; **10**: 2112–2118.
19. Wang Z, Ma H-I, Li J, Sun L, Zhang J, Xiao X. Rapid and highly efficient transduction by double-stranded adeno-associated virus vectors in vitro and in vivo. *Gene Ther* 2003; **10**: 2105–2111.
20. Niwa H, Yamamura K, Miyazaki J. Efficient selection for high-expression transfectants with a novel eukaryotic vector. *Gene* 1991; **108**: 193–200.
21. Nathwani AC, Gray JT, Ng CYC, *et al.* Self-complementary adeno-associated virus vectors containing a novel liver-specific human factor IX expression cassette enable highly efficient transduction of murine and nonhuman primate liver. *Blood* 2006; **107**: 2653–2661.
22. Matsushita T, Elliger S, Elliger C, *et al.* Adeno-associated virus vectors can be efficiently produced without helper virus. *Gene Ther* 1998; **5**: 938–945.
23. Okada T, Nomoto T, Shimazaki K, *et al.* Adeno-associated virus vectors for gene transfer to the brain. *Methods* 2002; **28**: 237–247.
24. Okada T, Nomoto T, Yoshioka T, *et al.* Large-scale production of recombinant viruses by use of a large culture vessel with active gassing. *Hum Gene Ther* 2005; **16**: 1212–1218.
25. Ishiwata A, Mimuro J, Mizukami H, *et al.* Liver-restricted expression of the canine factor VIII gene facilitates prevention of inhibitor formation in factor VIII-deficient mice. *J Gene Med* 2009; **11**: 1020–1029.
26. Lock M, McGorray S, Auricchio A, *et al.* Characterization of a recombinant adeno-associated virus type 2 reference standard material. *Hum Gene Ther* 2010; **21**: 1273–1285.
27. Kure S, Sato K, Fujii K, *et al.* Wild-type phenylalanine hydroxylase activity is enhanced by tetrahydrobiopterin supplementation in vivo: an implication for therapeutic basis of tetrahydrobiopterin-responsive phenylalanine hydroxylase deficiency. *Mol Genet Metab* 2004; **83**: 150–156.
28. Mochizuki S, Mizukami H, Kume A, *et al.* Adeno-associated virus (AAV) vector-mediated liver- and muscle-directed transgene expression using various kinds of promoters and serotypes. *Gene Ther Mol Biol* 2004; **8**: 9–18.
29. Ogura T, Mizukami H, Zhang YY, *et al.* Tissue distribution of expression using AAV8-based vectors after intramuscular injection and other routes of delivery. *Mol Ther* 2005; **11**: S334.
30. Ogura T, Mizukami H, Mimuro J, *et al.* Utility of intraperitoneal administration as a route of AAV serotype 5 vector-mediated neonatal gene transfer. *J Gene Med* 2006; **8**: 990–997.
31. Fang B, Eisensmith RC, Li XHC, *et al.* Gene therapy for phenylketonuria: phenotypic correction in a genetically deficient mouse model by adenovirus-mediated hepatic gene transfer. *Gene Ther* 1994; **1**: 247–254.
32. Pañeda A, Vanrell L, Mauleon I, *et al.* Effect of adeno-associated virus serotype and genomic structure on liver transduction and biodistribution in mice of both genders. *Hum Gene Ther* 2009; **20**: 908–917.
33. Vaessen SFC, Veldman RJ, Comijn EM, *et al.* AAV gene therapy as a means to increase apolipoprotein (Apo) A-I and high-density lipoprotein-cholesterol levels: correction of murine ApoA-I deficiency. *J Gene Med* 2009; **11**: 697–707.
34. Wu Z, Sun J, Zhang T, *et al.* Optimization of self-complementary AAV vectors for liver-directed expression results in sustained correction of hemophilia B at low vector dose. *Mol Ther* 2008; **16**: 280–289.
35. Nathwani AC, Cochrane M, McIntosh J, *et al.* Enhancing transduction of the liver by adeno-associated viral vectors. *Gene Ther* 2009; **16**: 60–69.
36. Nakai H, Fues S, Storm TA, Muramatsu S, Nara Y, Kay MA. Unrestricted hepatocyte transduction with adeno-associated virus serotype 8 vectors in mice. *J Virol* 2005; **79**: 214–224.
37. Nakai H, Yant SR, Storm TA, Fuess S, Meuse L, Kay MA. Extrachromosomal recombinant adeno-associated virus vector genomes are primarily responsible for stable liver transduction in vivo. *J Virol* 2001; **75**: 6969–6976.
38. Calos MP. The ΦC31 integrase system for gene therapy. *Curr Gene Ther* 2006; **6**: 633–645.
39. Ding Z, Harding CO, Rebuffat A, Elzaouk L, Wolff JA, Thöny B. Correction of murine PKU following AAV-mediated intramuscular expression of a complete phenylalanine hydroxylating system. *Mol Ther* 2008; **16**: 673–681.
40. Rebuffat A, Harding CO, Ding Z, Thöny B. Comparison of adeno-associated virus pseudotype 1, 2, and 8 vectors administered by intramuscular injection in the treatment of murine phenylketonuria. *Hum Gene Ther* 2010; **21**: 463–477.
41. Nathwani AC, Rosales C, McIntoh J, *et al.* Early clinical trial results following administration of a low dose of a novel self complementary adeno-associated viral vector encoding human factor ix in two subjects with severe haemophilia B. *Hum Gene Ther* 2010; **21**: 1362.

Cancer Science
The official journal of the Japanese Cancer Association JCA

Development of a mouse model for lymph node metastasis with endometrial cancer

Kayoko Takahashi,[1,2,4] Yasushi Saga,[2] Hiroaki Mizukami,[1,3] Yuji Takei,[2] Masashi Urabe,[1] Akihiro Kume,[1] Mitsuaki Suzuki[2] and Keiya Ozawa[1,3]

[1]Division of Genetic Therapeutics, Center for Molecular Medicine, Tochigi; [2]Department of Obstetrics and Gynecology, Jichi Medical University, Tochigi, Japan

(Received June 9, 2011/Revised September 5, 2011/Accepted September 5, 2011/Accepted manuscript online September 12, 2011/Article first published online October 17, 2011)

Controlling lymph node metastasis is currently a key issue in cancer therapy. Lymph node metastasis is one of the most important prognostic factors in various types of cancers, including endometrial cancer. Vascular endothelial growth factor-C (VEGF-C) plays a crucial role in lymphangiogenesis, and is implicated to play an important role in lymph node metastasis. To evaluate the role of VEGF-C in lymph node metastasis, we developed an animal model by using an endometrial cancer cell line, HEC1A. This cell line is not invasive by nature and secretes moderate amounts of VEGF-C; intrauterine injection of HEC1A cells into Balb/c nude mice resulted in uterine cancer with lymph node metastasis after 8 weeks. To analyze the contribution of VEGF-C to lymph node metastasis, its corresponding gene was stably introduced into HEC1A cells (HEC1A/VEGF-C), which then produced more than 10 times the amount of VEGF-C. The number of lymph node metastases was significantly higher in HEC1A/VEGF-C cells than in HEC1A cells (3.2 *vs* 1.1 nodes/animal, respectively). Augmented lymphangiogenesis was observed within tumors when HEC1A/VEGF-C cells were inoculated. These results indicate that VEGF-C plays a critical role in lymph node metastasis, in addition to serving as a platform to test the efficacy of various therapeutic modalities against lymph node metastasis. (*Cancer Sci* 2011; 102: 2272–2277)

Endometrial cancer is one of the most common gynecological malignancies, and the fourth most common malignancy.[1] The overall prognosis of endometrial cancer is considered to be better than that for other types of gynecological malignancies, because the disease can be detected in its early stages. However, the prognosis of patients with advanced stages of endometrial cancer is still poor, owing to the lack of effective treatment modalities. Furthermore, the overall survival rate for such patients has not improved over the past 30 years.[1] One of the most important prognostic factors in endometrial cancer is lymph node metastasis.[2,3] Therefore, it is vital to develop new treatment modalities that focus on lymph node metastasis.

The factors involved in lymphangiogenesis and lymph node metastasis were recently elucidated; it has become clear that vascular endothelial growth factor (VEGF)-C is a significant contributor.[4–6] Vascular endothelial growth factor-C is a 38-kDa glycoprotein that acts through a tyrosine kinase-type receptor, VEGF receptor 3 (VEGFR3). It is suggested that during malignancy, VEGF-C produced by tumor and/or interstitial cells promotes lymph node metastasis.[7] Vascular endothelial growth factor-C expression in uterine endometrial carcinoma was found to be related to both lymphatic vessel invasion and lymph node metastasis in a study with 228 surgical cases of endometrial cancer.[4]

The development of an adequate animal model is critical for facilitating research on lymph node metastasis. Therefore, we aim to develop a suitable animal model by using endometrial cancer cells.

Materials and Methods

Cells and plasmids. Human endometrial cancer cell lines, HEC1A and HEC50B, were obtained from the Japanese Collection of Research Bioresources; the cell lines were authenticated through the multiplex PCR method, using short tandem repeats,[8] and were maintained as described previously.[9,10] The Ishikawa cell line (clone 3H12) was a gift from Dr. M. Nishida (Department of Obstetrics and Gynecology, National Hospital Organization, Kasumigaura Medical Center, Ibaraki, Japan), and was maintained as described previously.[11] The VEGF-C sequence was obtained by PCR, using the following primer set against human placental cDNA: forward, 5′-ATGCACTTTGCTGGGCTTCTT-3′; reverse, 5′-CAATCTTAGCTCATTTGTGGTCT-3′. The VEGF-C expression plasmid, pCMV–VEGF-C–internal ribosome entry site (IRES)–blasticidin S-resistance (*bsr*) gene, was constructed by inserting the VEGF-C sequence into the *Eco*RI and *Xba*I sites of pCMV–IRES–*bsr*.[12]

Development of stably-transduced cells. The VEGF-C expression plasmid, pCMV–VEGF-C–IRES–*bsr*, and the control, pCMV–luciferase (LUC)–IRES–*bsr*,[12] were introduced into HEC1A cells by using the standard calcium phosphate method. The structures of these plasmids are shown in Figure 1. According to our previous experiments, introducing pCMV–LUC–IRES–*bsr* does not alter the growth, migration, invasive capacity, anticancer drug sensitivity, or the radiosensitivity of cells.[13]

Cells were selected in the presence of 10 μg/mL blasticidin S hydrochloride (Funakoshi, Tokyo, Japan) for 2 weeks, and the resistant cells were collected as HEC1A/VEGF-C and HEC1A/LUC.

Vascular endothelial growth factor-C quantification in culture supernatant. The culture medium was replaced by fresh medium without serum. After 48 h of culturing, the supernatants of each cell line (HEC1A, HEC1A/LUC, HEC1A/VEGF-C, HEC50B, and Ishikawa 3H12) were collected and subjected to VEGF-C analysis, using a Quantikine human ELISA kit (R&D Systems, Minneapolis, MN, USA).

***In vitro* cell growth kinetics.** The HEC1A, HEC1A/VEGF-C, and HEC1A/LUC cells were dispersed so that 1×10^5 cells were present in each well of 3.5-cm plastic dishes. After culturing, the cells were dislodged using 0.05% trypsin–EDTA every 24 h to determine the number of cells by using a hemocytometer.

***In vivo* tumor growth by subcutaneous inoculation.** Five- to 6-week-old female Balb/c nude mice (CLEA Japan, Tokyo, Japan) were used for the tumor growth experiments. All animal experiments were conducted according to the institutional and national guidelines for animal experiments. The HEC1A,

[3]To whom correspondence should be addressed.
E-mail: miz@jichi.ac.jp; kozawa@jichi.ac.jp
[4]Present address: The Cancer Institute Hospital of the Japanese Foundation for Cancer Research, Tokyo, Japan.

doi: 10.1111/j.1349-7006.2011.02099.x

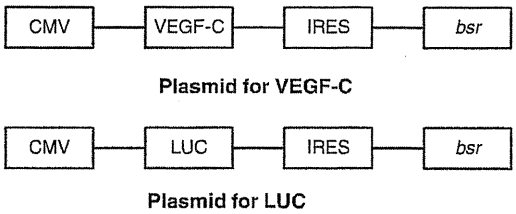

Fig. 1. Structure of the plasmids used in this study. Plasmids encoding vascular endothelial growth factor-C (VEGF-C) driven by the CMV promoter were used for cellular transduction. Plasmids encoding luciferase (LUC) were used as controls. *bsr*, blasticidin S-resistance gene; IRES, internal ribosome entry site.

HEC1A/VEGF-C, and HEC1A/LUC cells were implanted dorsally under the skins of the mice at 5×10^6 cells/site. Tumor volume was estimated using the formula: $0.5 \times L \times W^2$, where L and W indicate length and width in millimeters, respectively ($n = 5$).[14]

***In utero* transplantation of tumor cells.** Five- to 6- week-old female BALB/c nude mice (CLEA Japan) were used for the *in utero* experiments. A diagram of the injection procedure is shown in Figure 2. A laparotomy with a transverse incision was performed under general anesthesia, followed by ligation of the openings of the uterus at three locations, using 4-0 Vicryl (Ethicon, New Brunswick, NJ, USA). Tumor cells (5×10^6 cells) suspended in 50 μL PBS were injected into the uterine cavities by using a syringe with a 29-gauge needle. The left and right uterine cavities received similar volumes of cell suspension. The incisions were closed after the uterine tubes were inspected for proper enlargement and the absence of leakage. Uterine involvement and tumor development, especially lymph node metastasis, were evaluated periodically by laparotomy after the mice were killed.

Histological analysis of the animals. The animals were killed as scheduled, and all of the abdominal, thoracic, and retroperitoneal organs were inspected macroscopically. The metastatic lesions, uteri, and other organs showing possible signs of metastasis were microscopically evaluated for tumor progression. To estimate lymph node metastasis by size, recognizable lymph nodes were excised, and the presence of tumor metastasis was evaluated by histology in the first and second animal series. In the third and fourth animal series, the number of lymph node metastases was counted by enumerating lymph nodes larger than 3 mm in longitudinal diameter and evaluating them histologically.

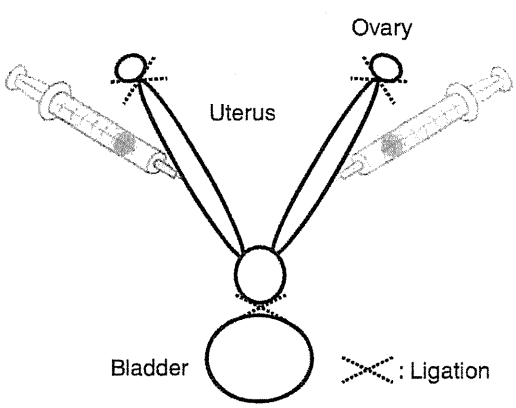

Fig. 2. Tumor cell injection procedure. After laparotomy under general anesthesia, all ends of the uterus were closed by ligation, ensuring the settlement of tumor cells within the uterine cavity. Following ligation, the cells were injected by puncturing the uterine wall. Abdominal incision was sutured after confirming that there was no leakage of cell suspension from the uterus.

Lymphangiogenesis in the subcutaneous tumor. At 2 weeks after the subcutaneous transplantation of corresponding cells (5×10^6 cells per animal) into the back, the mice ($n = 4$) were killed, and the subcutaneous tumors were excised. After fixation

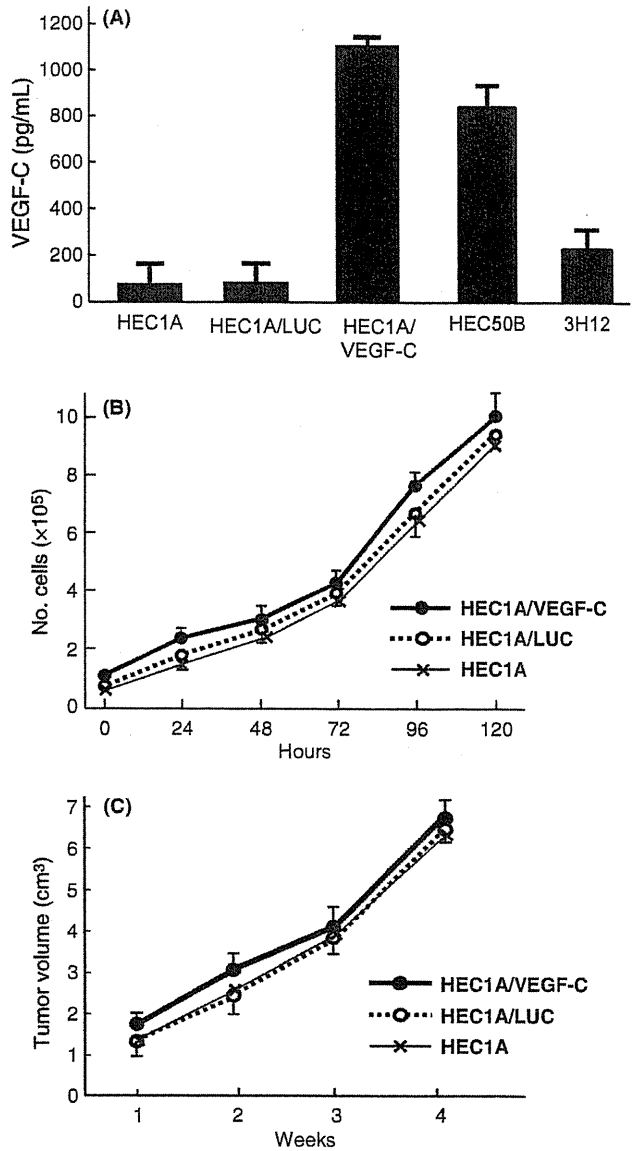

Fig. 3. (A) Vascular endothelial growth factor-C (VEGF-C)- or luciferase (LUC)-encoding plasmids were introduced into HEC1A cells by calcium phosphate transfection. Resultant cells were maintained, and the culture media were replaced with serum-free media upon confluence. After 48 h, the VEGF-C concentration of culture supernatants was determined by ELISA. Supernatant from the HEC1A/VEGF-C cells exhibited 10 times the concentration of VEGF-C, compared to the HEC1A or HEC1A/LUC cells. (B) Cells were dispersed at a concentration of 1×10^5/well in six well plates and were subsequently cultured. Cells were dislodged and counted after 24 h. There were no differences in the growth among these cell lines. (C) Growth of subcutaneous tumors after injection. Cells were subcutaneously injected into Balb/c nude mice (5×10^6 cells/site), and the tumor volumes were determined during follow up. No differences were found between these cells *in vivo*.

of the tumors in 4% paraformaldehyde, frozen sections were sliced, and antigen enhancement was done by heating the sections at 121°C in sodium citrate buffer (0.01 mol/L, pH 6.0) for 10 min, and endogenous peroxidase was blocked with 3% H_2O_2. The sections were incubated overnight at 4°C with a 1:500 dilution of anti-VEGFR3 antibody (Abcam, Cambridge, UK) as the primary antibody recognizing lymphatic endothelial cells, and then reacted with the secondary antibody, that is, the peroxidase-conjugated antirat antibody (Simple Stain Mouse MAX-PO, Rat; Nichirei, Tokyo, Japan) at room temperature for 30 min, followed by color development with diaminobenzidine. The number of newly-formed lymph vessels was counted under a light microscope at ×20 magnification. A single section was prepared per mouse in four animals per group, and new lymph vessels were counted in the four sections and averaged.

Verification. All *in vitro* experiments were performed at least three times.

Results

***In vitro* production of VEGF-C and cell growth kinetics.** Culture supernatants of the HEC1A and HEC1A/LUC cells showed similar VEGF-C concentrations, whereas the HEC1A/VEGF-C cells produced much greater concentrations of VEGF-C (Fig. 3A). There were no differences in the growth properties of the HEC1A/LUC and HEC1A/VEGF-C cells, both *in vitro* and *in vivo* (Fig. 3B,C).

***In vivo* transplantation of tumor cells.** When the HEC1A/LUC cells were injected into the uterus, subsequent tumor development was observed; therefore, follow ups were performed to determine the occurrence of lymph node metastases (Table 1). At 4 weeks, one of five mice developed metastasis; at 6 weeks, two of four developed metastasis. At 8 weeks after injection, all of the mice in the first series exhibited lymph node metastasis. Consequently, the second series was carried out using a larger number of animals, which again resulted in the successful development of metastases within the same time frame. At 8 weeks, the uterus was swollen and the endometrium was filled with tumor cells (Fig. 4A,B). Marked infiltrations into the enlarged lymph nodes were also noted in mice injected with the HEC1A/LUC (Fig. 4C) and HEC1A/VEGF-C (Fig. 4D,E) cells.

Relationship between lymph node size and metastasis. Upon analysis of the model mice, 40 lymph nodes were selected by size and excised for histological evaluation. Lymph nodes larger than 3 mm in longitudinal diameter were all positive for tumor metastasis, whereas smaller ones exhibited lower positivity (Fig. 5A).

Effect of VEGF-C on lymph node metastasis. The results of the third and fourth series revealed a significant increase in the number of metastases when VEGF-C was overexpressed by the cells (1.1 ± 0.8 *vs* 3.2 ± 1.3, third and fourth series, respectively). Statistical significance was determined by the Mann-Whitney *U*-test (Fig. 5B).

Reproducibility of lymph node metastasis. As shown in Table 1, the majority of animals developed lymph node metastasis at 8 weeks after injection. The overall rate of positive lymph node metastasis was 86.5% (45/52 animals). All lymph nodes >3 mm in longitudinal diameter contained tumor cells, as determined by histological analysis (Fig. 5B). No animals exhibited direct invasion of the tumor or metastatic lesions other than the lymph nodes.

Lymphangiogenesis in the subcutaneous tumor. After 2 weeks of subcutaneous inoculation, the tumors were analyzed histochemically. The tumor tissue based on the HEC1A/VEGF-C cells exhibited a marked increase in VEGFR3-positive vessels compared with the HEC1A/LUC cells (Fig. 6A,B). The number

Table 1. Number of animals with lymph node metastasis

Weeks	4	6	8
First series (HEC1A/LUC)	1/5	2/4	4/4
Second series (HEC1A/LUC)	–	–	8/8
Third series (HEC1A/LUC)	–	–	15/21
Fourth series (HEC1A/VEGF-C)	–	–	18/19

HEC1A, an endometrial cancer cell line; LUC, luciferase; VEGF-C, vascular endothelial growth factor-C.

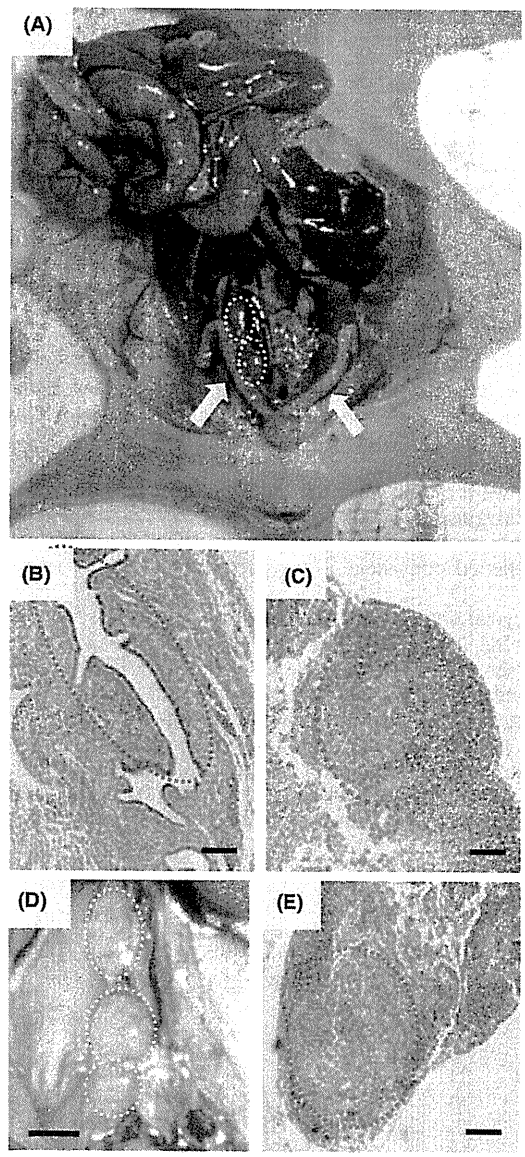

Fig. 4. Involvement of cancer cells *in vivo*, 8 weeks after injection. (A–C) animals were injected with HEC1A/luciferase cells. (A) Enlarged uterus (arrows) and lymph nodes (dotted circles) are shown. No other metastatic sites were found in these animals. (B) Micrograph of a uterus. Tumor cells in the endometrial zone, which resemble a uterus with endometrial cancer. (C) Enlarged lymph node with tumor metastasis. (D) Para-aortic lymph node swelling was observed in mice injected with HEC1A/vascular endothelial growth factor-C cells. Dotted circles indicate enlarged lymph nodes. (E) Lymph node metastasis was confirmed by histological evidence of tumor infiltration. Bars in (B), (C), and (E) indicate 1 mm; bar in (D) indicates 4 mm.

doi: 10.1111/j.1349-7006.2011.02099.x

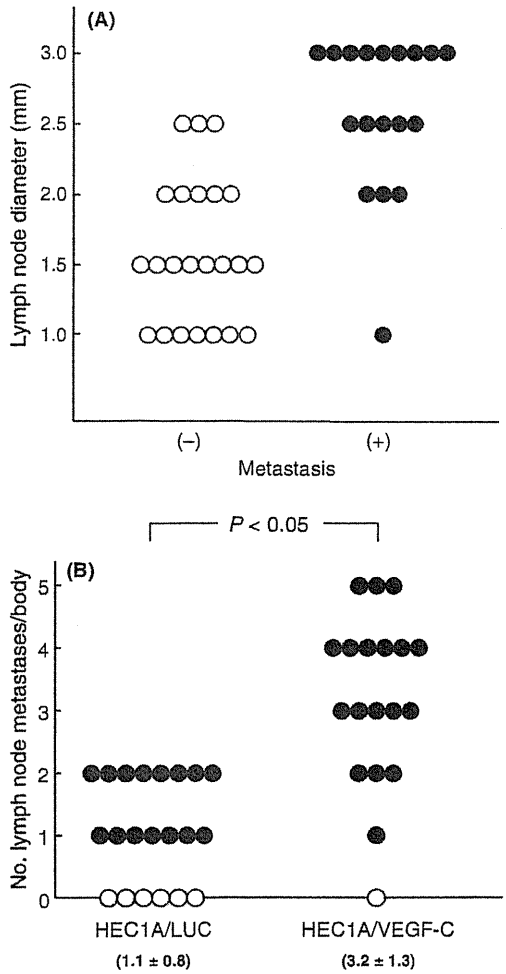

Fig. 5. Number of lymph nodes in animals, 8 weeks after tumor injection. (A) Relationship between lymph node size (longitudinal diameter) and metastasis is shown. Closed circles indicate histologically-positive metastasis. (B) Number of metastatic lymph nodes larger than 3 mm in longitudinal diameter at 8 weeks. Results from the third and fourth series are shown. Closed circles indicate histologically-positive metastasis. Animals injected with HEC1A/vascular endothelial growth factor-C (VEGF-C) showed a higher number of lymph node metastases. LUC, luciferase.

of VEGFR3-positive vessels in each group (n = 4) were counted using microscopy, and the results were analyzed. A significant increase was observed in tumors originated from HEC1A/VEGF-C cells (Student's t-test, Fig. 6C).

Discussion

In the present study, we developed a unique lymph node metastasis model by orthotopically injecting endometrial cancer cells. In this method, most of the animals exhibited lymph node metastasis, along with uterine involvement in cancer. The reproducibility of the metastases seen in our experiment is extremely

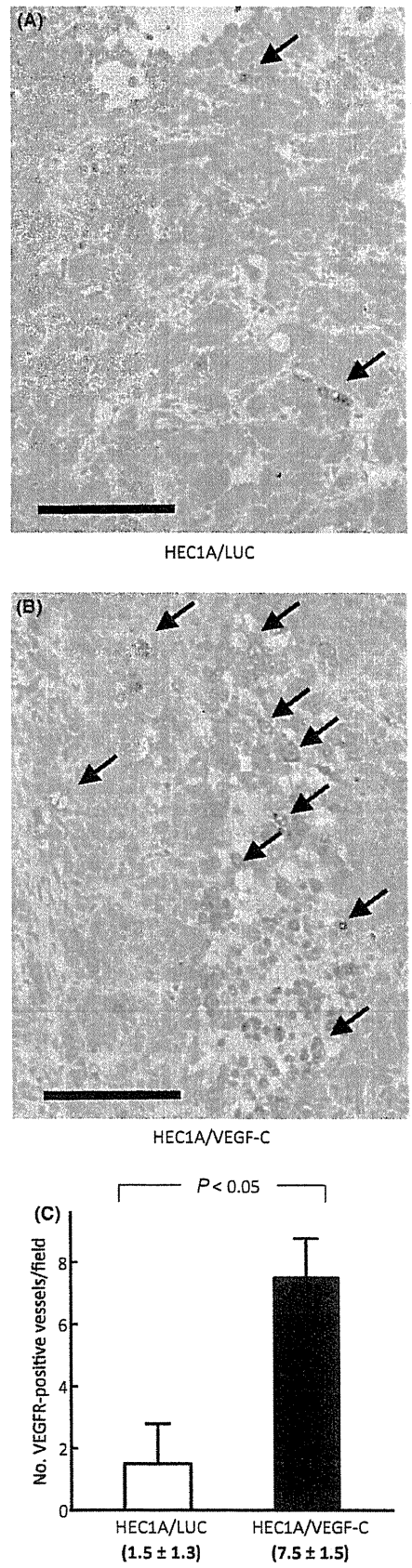

Fig. 6. Immunohistochemical analysis of subcutaneously-inoculated tumor. Arrows indicate vascular endothelial growth factor (VEGF) receptor 3 (VEGFR3)-positive vessels, possibly reflecting lymphangiogenesis in HEC1A/luciferase (LUC) (A) and HEC1A/VEGF-C cells (B). Bars indicate 100 μm. (C) Number of vessels positive for VEGFR3 was enumerated under a light microscope at ×20 magnification. Four animals were used for each cell.

important in developing a model for lymph node metastasis. In our model, all animals survived the injection procedure, and 45 of 52 mice (86.5%) exhibited positive lymph node metastasis. This rate is remarkably high, thus making this model reliable for further therapeutic interventions. In all of the animals, uterine tumor growth was local and self-limited, and the peritoneal dissemination of other sites of metastasis was not evident. These features considerably reflect the clinical conditions of lymph node metastasis, assuring the utility of the model.

Nonetheless, when the present pathological findings are compared to those of human cases, there are slight differences in the metastatic regions. In the mice used in the present experiments, only para-aortic lymph node areas were involved, whereas in humans, pelvic lymph nodes are also metastasized. While this difference might be due to differences in lymphatic anatomy, it would be advantageous for researchers to evaluate metastatic conditions more clearly.

There are a number of decisions to be made when developing models, such as choosing cell lines, the number of cells for injection, various technical details, and observation periods. We initially selected HEC1A cells, because they are one of the most widely used endometrial cancer cell lines. Based on our experience, HEC1A cells appeared to be the most suitable for the present study; lymph node metastasis was well developed before other potential metastatic sites or original growths. One of the most important aspects is the invasiveness of the cells. HEC1A cells are not very invasive by nature, and did not cause peritoneal dissemination in our series of experiments during the observation period. In fact, we also tested HEC50B cells and found that although metastatic lesions were found earlier (by 4–5 weeks), tumor invasion into the surrounding areas was prominent, and consequently, the animals were not suitable for further evaluation of metastasis. The invasiveness seems unrelated to the levels of VEGF-C production, but related to the state of differentiation. HEC1A cells are known to be well differentiated, whereas HEC50B cells are poorly differentiated. In this respect, Ishikawa (3H12) cells might be a good candidate, as they are classified as well-differentiated carcinoma; nonetheless, they are also known to transform into undifferentiated status under prolonged culture.[11] For this reason, we did not test this cell line for the development of the model.

The number of cells per injection is another important factor when developing a model. As a general rule, the more cells that are injected, the earlier the disease develops. The number of cells used in this study (5×10^6) was near maximum, because the least amount of solution to suspend the cells is close to the maximum volume for intrauterine injections in BALB/c mice (approximately 80 μL). It is also imperative to keep the tumor cells within the uterine cavity after injection. To do so, it is important that the distal ends of the uterus and cervix are appropriately ligated, while avoiding excessive amounts of injection. If the cells flow out from the distal end of the uterus, they might spread into the peritoneal space, leading to intraperitoneal tumor dissemination. Alternatively, if the cells are lost through the vagina, the inoculation is deemed unsuccessful. In our experiments, no significant intraperitoneal regions were observed in the animals, even when lymph node metastases were not evident.

Two previous studies established lymph node metastasis models by injecting cancer cells into the uterus. The first study utilized the metastatic subline PL3 of rat Walker 256 cells.[15] This cell line originates from mammary tumor cells, and the metastatic subline was enriched after more than five cycles of *in vivo* selection. Another study orthotopically implanted MH and KF cells; both originate from human ovarian cancer.[16] The latter study also established highly metastatic sublines (MH–LN3 and KF–LN3) after three cycles of *in vivo* selection. Therefore, the *in vivo* selection of the cells is essential before establishing a metastasis model. Meanwhile, the stability of the metastatic sublines, along with their availability, is not clear. In this study, we utilized publicly-available cell lines without *in vivo* selection steps. These features, along with the high rate of reproducibility, make this model particularly useful for evaluating lymph node metastasis.

At the time of histological evaluation, various sizes of lymph nodes were found, and it was difficult to estimate whether they were metastatic or not. To simplify the evaluation steps, we tested for the presence of metastatic tumors in lymph nodes by size. As shown in Figure 5(A), all lymph nodes larger than 3 mm were positive for metastasis. Therefore, we enumerated lymph nodes by using this size limit. In addition, the lymph nodes shown in Figure 5(B) were also analyzed; the additional 84 lymph nodes were all positive for metastasis. With these results, we are confident that we can estimate the metastasis solely by the size of the lymph node, at least in this model.

Based on our results, it is clear that the overexpression of VEGF-C results in an enhancement of lymph node metastasis (Fig. 5B). The use of this particular cell line results in a more robust model for lymph node metastasis. It is very likely that the activity of VEGF-C secreted from the tumors facilitates lymph node metastasis. In the present study, we demonstrated significant increase of VEGFR3-positive vessels within the tumor, suggesting enhanced lymphangiogenesis by VEGF-C (Fig. 6). The precise mechanism of VEGF-C, with regard to lymph node metastasis, is not well understood; few existing studies focus on this point. One study suggests that lymphatic endothelial cell (LEC) migration, rather than proliferation, is responsible for metastasis in pancreatic cell lines.[17] In that study, the relationship between VEGF-C concentration and the number of migrating LEC exhibited a positive but non-linear correlation; this is quite similar to our observation between VEGF-C and the number of lymph node metastases. In any case, it is expected that blocking the activity of VEGF-C would suppress lymph node metastasis. We are currently preparing a therapeutic experiment that incorporates soluble VEGFR3 into this model.

The prognosis of endometrial carcinoma with lymph node metastasis is poor, and few improvements have been made. The present model might offer a platform on which therapeutic progress against lymph node metastasis can be made.

Acknowledgments

This study was supported in part by grants from Ministry of Health, Labor and Welfare, Japan, and the Ministry of Education, Culture, Sports, Science, and Technology, Japan.

Disclosure Statement

The authors declare no financial or commercial conflict of interest.

References

1 Jemal A, Siegel R, Xu J, Ward E. Cancer statistics, 2010. *CA Cancer J Clin* 2010; **60**: 277–300.

2 Lurain JR, Rice BL, Rademaker AW, Poggensee LE, Schink JC, Miller DS. Prognostic factors associated with recurrence in clinical stage I adenocarcinoma of the endometrium. *Obstet Gynecol* 1991; **78**: 63–9.

3 Wolfson AH, Sightler SE, Markoe AM *et al.* The prognostic significance of surgical staging for carcinoma of the endometrium. *Gynecol Oncol* 1992; **45**: 142–6.

4 Hirai M, Nakagawara A, Oosaki T, Hayashi Y, Hirono M, Yoshihara T. Expression of vascular endothelial growth factors (VEGF-A/VEGF-1 and VEGF-C/VEGF-2) in postmenopausal uterine endometrial carcinoma. *Gynecol Oncol* 2001; **80**: 181–8.

doi: 10.1111/j.1349-7006.2011.02099.x

5 Makinen T, Veikkola T, Mustjoki S *et al.* Isolated lymphatic endothelial cells transduce growth, survival and migratory signals via the VEGF-C/D receptor VEGFR-3. *EMBO J* 2001; **20**: 4762–73.
6 Mandriota SJ, Jussila L, Jeltsch M *et al.* Vascular endothelial growth factor-C-mediated lymphangiogenesis promotes tumour metastasis. *EMBO J* 2001; **20**: 672–82.
7 Skobe M, Hawighorst T, Jackson DG *et al.* Induction of tumor lymphangiogenesis by VEGF-C promotes breast cancer metastasis. *Nat Med* 2001; **7**: 192–8.
8 Tanabe H, Takada Y, Minegishi D, Kurematsu M, Masui T, Mizusawa H. Cell line individualization by STR multiplex system in the cell bank found cross contamination between ECV304 and EJ-1/T24. *Tiss Cult Res Commun* 1999; **18**: 329–38.
9 Kuramoto H, Tamura S, Notake Y. Establishment of a cell line of human endometrial adenocarcinoma *in vitro*. *Am J Obstet Gynecol* 1972; **114**: 1012–9.
10 Suzuki M, Kuramoto H, Hamano M, Shirane H, Watanabe K. Effects of oestradiol and progesterone on the alkaline phosphatase activity of a human endometrial cancer cell-line. *Acta Endocrinol (Copenh)* 1980; **93**: 108–13.
11 Nishida M. The Ishikawa cells from birth to the present. *Hum Cell* 2002; **15**: 104–17.
12 Urabe M, Hasumi Y, Ogasawara Y *et al.* A novel dicistronic AAV vector using a short IRES segment derived from hepatitis C virus genome. *Gene* 1997; **200**: 157–62.
13 Takei Y, Mizukami H, Saga Y *et al.* Suppression of ovarian cancer by muscle-mediated expression of soluble VEGFR-1/Flt-1 using adeno-associated virus serotype 1-derived vector. *Int J Cancer* 2007; **120**: 278–84.
14 Kung AL, Wang S, Klco JM, Kaelin WG, Livingston DM. Suppression of tumor growth through disruption of hypoxia-inducible transcription. *Nat Med* 2000; **6**: 1335–40.
15 Hashii K, Tohya K, Kimura M *et al.* Novel animal model of lymph node metastasis by intrauterine inoculation of the actively metastatic subline PL3 separated from rat Walker 256 tumor cells. *Invasion Metastasis* 1997; **17**: 149–57.
16 Tamada Y, Aoki D, Nozawa S, Irimura T. Model for paraaortic lymph node metastasis produced by orthotopic implantation of ovarian carcinoma cells in athymic nude mice. *Eur J Cancer* 2004; **40**: 158–63.
17 Ochi N, Matsuo Y, Sawai H *et al.* Vascular endothelial growth factor-C secreted by pancreatic cancer cell line promotes lymphatic endothelial cell migration in an *in vitro* model of tumor lymphangiogenesis. *Pancreas* 2007; **34**: 444–51.

Journal of Stem Cells & Regenerative Medicine
ISSN 0973 - 7154

RESEARCH ARTICLE

JSRM Code: 007020300010

Reciprocal upregulation of Notch signaling molecules in hematopoietic progenitor and mesenchymal stromal cells

Kikuchi Y[1,2], Kume A[2*], Urabe M[2], Mizukami H[2], Suzuki T[1], Ozaki K[1], Nagai T[1], Ozawa K[1,2]

Although mesenchymal stem cells (MSCs) play pivotal supportive roles in hematopoiesis, how they interact with hematopoietic stem cells (HSCs) is not well understood. We investigated the interaction between HSCs and surrogate MSCs (C3H10T1/2 stromal cells), focusing on the molecular events induced by cell contact of these bipartite populations. C3H10T1/2 is a mesenchymal stromal cell line that can be induced to differentiate into preadipocytes (A54) and myoblasts (M1601). The stromal cell derivatives were cocultured with murine HSCs (Lineage$^-$Sca1$^+$), and gene expression profiles in stromal cells and HSCs were compared before and after the coculture. HSCs gave rise to cobblestone areas only on A54 cells, with ninefold more progenitors than on M1601 or undifferentiated C3H10T1/2 cells. Microarray-based screening and a quantitative reverse transcriptase directed-polymerase chain reaction showed that the levels of Notch ligands (Jagged1 and Delta-like 3) were increased in A54 cells upon interaction with HSCs. On the other hand, the expression of Notch1 and Hes1 was upregulated in the HSCs cocultured with A54 cells. A transwell assay revealed that the reciprocal upregulation was dependent on cell-to-cell contact. The result suggested that in the hematopoietic niche, HSCs help MSCs to produce Notch ligands, and in turn, MSCs help HSCs to express Notch receptor. Such a reciprocal upregulation would reinforce the downstream signaling to determine the fate of hematopoietic cell lineage. Clarification of the initiating events on cell contact should lead to the identification of specific molecular targets to facilitate HSC engraftment in transplantation therapy.

Introduction

Hematopoietic stem cells (HSCs) are capable of self-renewing and differentiating into all the blood cell lineages, and the property allows them to reconstitute adult hematopoiesis following transplantation. The growth and differentiation of HSCs is regulated by orchestrated signals from various soluble factors and the hematopoietic microenvironment, or 'niche'. With the aid of many other cell types, osteoblasts and vascular endotherial cells maintain the balance of dormant and active HSCs in the osteoblasic and vascular niches [1-4].

The interaction between HSCs and the niche cells comprises cytokines and cell-to-cell contact. The involved cytokines include stem cell factor (SCF), stromal-derived factor 1 (SDF1), angiopoietin1 (Ang1) and osteopontin, and the functions of these factors have been studied extensively [5-9]. On the other hand, molecular events of the direct cell contact are mostly unclear. Wagner et al. investigated the behavioral and molecular changes in hematopoietic progenitors upon interaction with a stromal cell line AFT024 [10]. They found that the genes involved in the cytoskeleton reorganization, DNA stabilization and methylation were upregulated. However, molecular events in the niche cells have not vigorously explored.

Mesenchymal stem cells (MSCs) in the bone marrow play a vital role in supporting hematopoiesis, therefore they are considered as niche cells, too [11,12]. To further explore the hematopoiesis-supporting ability of MSCs, we have used a surrogate MSC line C3H10T1/2 (10T1/2) and its derivative preadipocytes (A54) and myoblasts (M1601). Among these cells, only A54 preadipocytes helped the expansion of hematopoietic progenitors with an augmented production of SCF, SDF1 and Ang1 [13,14]. In the present study, we investigated the cellular and molecular events in the interactive communication between HSCs and stromal cells using this differentiation-inducible system, particularly focusing on the changes in the stromal cells.

Materials and methods

Cells

10T1/2 cell line (from Riken Biological Resource Center, Tsukuba, Japan) was used as an inducible MSC model. A54 preadipocytes and M1601 myoblasts were established as described previously [13]. All the cell lines were cultured in Iscove's Modified Dulbecco's Medium (Invitrogen, Carlsbad, CA, USA) supplemented with 10% fetal bovine serum (FBS; Sigma, St. Louis, MO, USA). Bone marrow mononuclear cells were separated from C57BL/6 mouse femurs using

[1]Division of Hematology, Department of Medicine, Jichi Medical University, Shimotsuke, Tochigi, Japan.
[2]Division of Genetic Therapeutics, Center for Molecular Medicine, Jichi Medical University, Shimotsuke, Tochigi, Japan.

Received 02 Jun; accepted 23 Jul; published online 30Oct 2011